

# Analysis and modeling of epithelial tissue organization during head involution stage of *Drosophila* embryogenesis



A thesis submitted towards the partial fulfillment of  
BS-MS dual degree programme  
from June 2017 to February 2018

by

ABHISHEK DAS  
BS-MS 20131056


under the guidance of

DR CHAITANYA ATHALE  
ASSOCIATE PROFESSOR  
INDIAN INSTITUTE OF SCIENCE EDUCATION AND RESEARCH, PUNE


DR JEROME SOLON  
GROUP LEADER  
CENTRE FOR GENOMIC REGULATION, BARCELONA

# Certificate

This is to certify that this dissertation entitled "Analysis and modeling of epithelial tissue organization during head involution stage of *Drosophila* embryogenesis" submitted towards the partial fulfillment of the BS-MS degree at the Indian Institute of Science Education and Research, Pune represents original research carried out by "Abhishek Das" at "Indian Institute of Science Education and Research, Pune and Centre for Genomic Regulation, Barcelona", under the supervision of "Dr Chaitanya Athale and Dr Jerome Solon" during academic year June 2017 to February 2018.



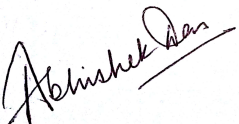
Student  
ABHISHEK DAS  
BS-MS 20131056

Supervisor   
CHAITANYA ATHALE  
ASSOCIATE PROF.  
IISER, PUNE  
DATE: 29/03/2018

Supervisor  
JEROME SOLON  
GROUP LEADER  
CRG BARCELONA  
DATE: / / 30/03/2018

# Declaration

I, hereby declare that the matter embodied in the report titled “Analysis and modeling of epithelial tissue organization during head involution stage of *Drosophila* embryogenesis” is the results of the investigations carried out by me at the Indian Institute of Science Education and Research, Pune and Centre for Genomic Regulation, Barcelona under the supervision of Dr Chaitanya Athale and Dr Jerome Solon and the same has not been submitted elsewhere for any other degree.



Student  
ABHISHEK DAS  
BS-MS 20131056



Supervisor  
CHAITANYA ATHALE  
ASSOCIATE PROF.  
IISER PUNE  
DATE: 29/03/2018

Supervisor  
JEROME SOLON  
GROUP LEADER  
CRG BARCELONA  
DATE: / / 30/03/2018

# Acknowledgements

I would like to thank all the people associated with this project especially Neha Khetan, Anushree Chaphalkar, Kunalika Jain, Arturo D'Angelo, Dr Amelie Godeau, Dr Alba Granados for the constant help and support, Dr Pranay Goel for being in my thesis advisory committee and suggesting useful inputs and most importantly, Dr Chaitanya Athale and Dr Jerome Solon for mentoring me in developing a scientific temper throughout this project. Last but not the least I would like to thank my parents, Mr. Ajay Day and Mrs. Tulu Das, and my sister Mrs. Indrani Das Rakshit, brother-in-law Mr. Gautam Rakshit for always being my constant source of inspiration and guiding me in my endeavours.

# Abstract

Tissue biomechanics plays an important role in the progression of epidermal tissue during the head involution process of *Drosophila* embryogenesis. Understanding the self-organizing principles which are controlling the underlying segment width control by modulations in the cellular shape pattern in such epithelial tissue spreading is necessary for identifying crucial factors in cell migration, tissue growth, and regeneration. We try to corroborate our experimental observations about pattern of periodic cell shapes and equal tissue segment width at the completion of the involution process with a 2D tissue simulation setup using the Cellular Potts model (CPM). The model partially manages to recover some of the experimental data using only the physical parameters of cortical tension along with providing an explanation for the variation in cell shapes and segment width seen in WT embryos. Further, following from previous published data, a correlation between Hh genes and junctional tension at the segmental boundary regions of the epithelial tissue organization during the head involution stage of embryogenesis can be modelled by incorporation of biochemical feedback into the CPM model. Implementation of a diffusion gradient of Hh and Wg incorporated with the cell mechanics of the Potts model is hypothesized to validate the findings of patterned contractile forces at the global tissue scale reported previously by Czerniak et al [2016](#).

# Contents

<b>1</b>	<b>Introduction</b>	<b>4</b>
1.1	Biomechanics of epithelial tissue morphogenesis . . . . .	4
1.1.1	Existing methods of understanding tissue organization and morphogenesis . . . . .	4
1.2	Epithelial spreading: head involution (HI) in <i>Drosophila melanogaster</i> . . . . .	6
1.2.1	Relevancy of studying involution phenomenon . . . . .	6
1.3	Genetic regulation of tissue mechanics at intrasegmental boundaries . . . . .	7
1.3.1	Role of Hedgehog (Hh) signaling in segment positioning . . . . .	7
1.4	1D Elastic epidermal sheet . . . . .	8
1.5	Understanding segment width and cell shapes during involution process . . . . .	9
<b>2</b>	<b>Model</b>	<b>10</b>
2.1	Elastic tissue simulation based on CPM formalism . . . . .	10
2.2	Effective model of morphogen diffusion . . . . .	11
<b>3</b>	<b>Methods</b>	<b>13</b>
3.1	Simulation Methods . . . . .	13
3.1.1	Pott's model in CompuCell3D platform . . . . .	13
3.1.2	Observation of segment positioning by regulation of cortical tension ( $\gamma_s$ ) and surface tension ( $\gamma_v$ ) parameters . . . . .	14
3.1.3	Measures of cell shapes . . . . .	15
3.1.4	Voronoi tessellation using delaunay algorithm . . . . .	16
3.1.5	Reaction-Diffusion solvers . . . . .	16
3.2	Experimental Methods . . . . .	17
3.2.1	<i>Drosophila</i> embryo preparation and microscopy . . . . .	17
3.2.2	Image processing . . . . .	17
<b>4</b>	<b>Results</b>	<b>19</b>
4.1	Experimental Results . . . . .	19
4.1.1	Progression of epithelial tissue during head involution . . . . .	19
4.1.2	Tissue segmentation after completion of HI . . . . .	21
4.1.3	Unequal segment width in overexpressed-Hh embryos . . . . .	22
4.2	Simulation Results . . . . .	22
4.2.1	Effect of differential adhesion energy between cell-cell junctions . . . . .	22
4.2.2	Effect of embryonic geometry on tissue cell shapes . . . . .	24
4.2.3	Interplay of cortical and surface tension regulates cell shapes . . . . .	26
4.2.4	Recapitulation of overexpressed-Hh data in simulation setup . . . . .	27

4.2.5	Organisation of tissue segments using bands of a contractile ring of cells . . . . .	27
4.3	Incorporation of morphogen gradient . . . . .	30
<b>5</b>	<b>Discussion and Conclusion</b>	<b>35</b>
	<b>Bibliography</b>	<b>37</b>

# List of Figures

1.1	Asymmetries in force-generating mechanisms in tissues . . . . .	5
1.2	Robust segment-polarity gene network model . . . . .	6
1.3	Distribution of epidermal segments . . . . .	7
1.4	1D Elastic epidermal sheet models . . . . .	8
2.1	Intra-segmental morphogen gradient scheme . . . . .	12
3.1	Modelling in CC3D . . . . .	13
3.2	Fixed elliptical geometry . . . . .	14
3.3	Simulation setup with six segments . . . . .	15
3.4	Protocol for experiment . . . . .	18
4.1	Time lapse snapshots of <i>Drosophila</i> embryos . . . . .	20
4.2	Denticle tracking . . . . .	21
4.3	Tissue segmentation of WT embryos . . . . .	23
4.4	Polygonal approximation of tissue cells . . . . .	24
4.5	Differential Adhesion Hypothesis schematic . . . . .	25
4.6	Periodic square boundary setup . . . . .	25
4.7	Steady-state nature of circularity . . . . .	26
4.8	Larger cell system . . . . .	27
4.9	Voronoi analysis of larger system . . . . .	28
4.10	Smaller cell system analysis . . . . .	29
4.11	Regulation of cortical tension in cell shape analysis . . . . .	30
4.12	Recapitulation of ovr-Hh data in simulation . . . . .	31
4.13	Bands of contractile cells . . . . .	32
4.14	1D morphogen gradient simulation over space and time . . . . .	33
4.15	Reaction-diffusion model of morphogens in secreting cells . . . . .	34
5.1	Anisotropic nature of cortical forces . . . . .	36
5.2	3D embryo model in CC3D . . . . .	37



# Chapter 1

## Introduction

All life began as a single cell and grew to a blastula of cells, before forming all the shapes seen in nature (Karsenti 2008). The shape and size of cellular systems are of fundamental importance to their function and has been explained by equilibrium mechanics of soap bubbles previously (Thompson 1942). Generation of forces by the cytoskeletal elements which includes the acto-myosin mesh (Salbreux *et al.* 2012) as well as biochemical changes caused by signal transduction channels (e.g., Rac-RhoA dynamics) (Marée *et al.* 2012) and the response of the cell to such mechanical and chemical loads gives rise to the process of cellular morphogenesis (Lecuit and Lenne 2007). However, with recent insights into genetics, one also needs to consider the intricate and complex cell fate governing epigenetic factors that also plays a role in morphogenesis (Müller and Newman 2003).

### 1.1 Biomechanics of epithelial tissue morphogenesis

Epithelia are layered sheets of cells that line the cavities and outer surfaces of the animal body, and constitute one of the four basic types of animal tissues. The development of the epithelial junctional network in *Drosophila melanogaster* is tightly controlled by packing geometries of cells which depends on their interactions with other cells (Fig.1.1). Mechanical forces including elastic spring-like forces play an essential role in tissue development. These tissues can be thought of as some soft material, with latent elasticity variables of Young's and Bulk modulus, which shows bending and thinning under contractile and expanding forces. Non-uniform deformation is observed through the tissue structure under compression. The chemical makeup of these tissues contributes to the global scale material properties of the epithelial tissue. Production of forces in the highly viscous environments is a necessary criterion for cells to move around and they do so in different ways characterized by various molecular as well as physiological processes.

#### 1.1.1 Existing methods of understanding tissue organization and morphogenesis

To understand these type of epithelial tissue organization, two main approaches have been followed traditionally: 1) Vertex Model (Farhadifar *et al.* 2007) 2) Pott's Model. The dominating factors determining cell and tissue shapes are the elasticity of the cells and junctional tension which are results of the contractile nature of the cytoskeletal components and the adhesion forces (Fletcher *et al.* 2013). Although both these models account for the above mentioned forces, the vertex model follows hexagonal packing

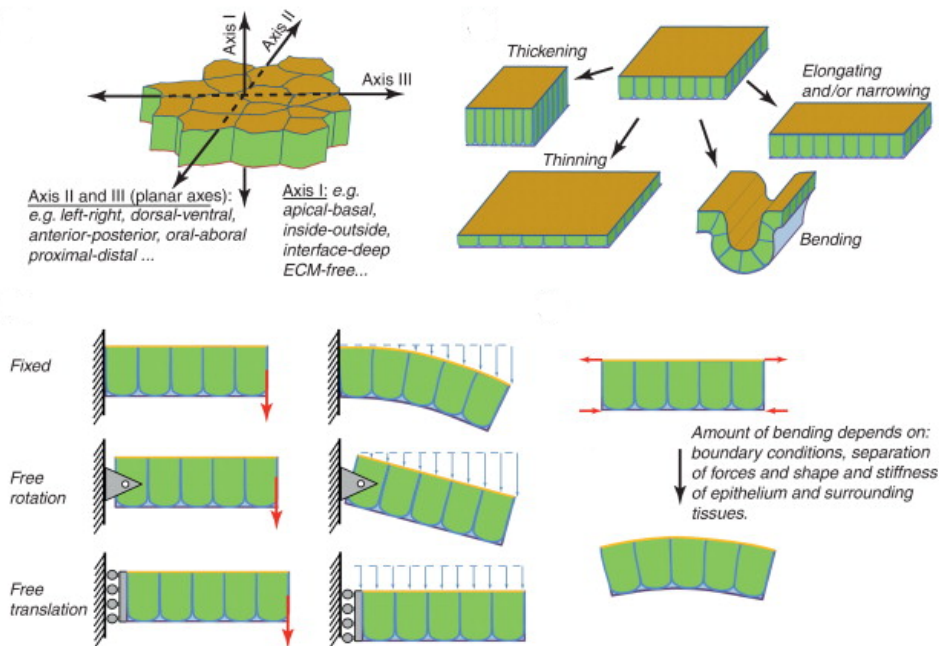


**Figure 1.1:** Asymmetries in force-generating mechanisms due to constraining boundary conditions can alter epithelial cell packing in tissues; The rigidity constants of the tissue material along with proper boundary value conditions regulate movement of 2D like elastic sheet of cells; Adapted from Davidson 2012

analysis while the Pott's model is based on the cell sorting by Differential Adhesion Hypothesis (Steinberg 2007).

Vertex models (Farhadifar *et al.* 2007) are based on foundations of nodes from graph theory in mathematics and Boltzmann weighting factors from statistical mechanics in physics wherein geometries of the cell shape are characterized by pre-existing nodes and edges and the cell shape is predicted beforehand on the basis of such kind of possible and probable combinations of the nodes. Although these models could explain tissue morphogenesis at the bulk level quite nicely the inherent assumption about a prediction of cell shape remains and as such a need is there of more robust models which don't take into account the assumption of pre-existing cell shape.

Hence, we turn to energy based models from statistical mechanics where dynamics can be studied regarding the state of the system at that point in time (Procacci *et al.* 2016). These models are randomized and are wholly based on the energy of the state without any assumption of about the shape or directionality of the cell beforehand. One such model that we will be discussing in detail is the Cellular Potts Model (Turner *et al.* 2004, Niculescu *et al.* 2015) which is a variant of the famous Ising model in statistical mechanics to explain the spin properties of metallic conductors. Francois Graner and James Glazier proposed an extended Cellular Pott's model which could be used in biology to characterize cell sorting (Graner and Glazier 1992), cell morphogenesis and cell migration on the basis on volume and surface constraint properties of the cells. The most desirable characteristic such energy-based models put forward is that the possibility of combining the mechanistic aspects of the cell morphogenesis coupled to the biochemical feedback signaling pathways becomes an exciting prospect of study.

## 1.2 Epithelial spreading: head involution (HI) in *Drosophila melanogaster*

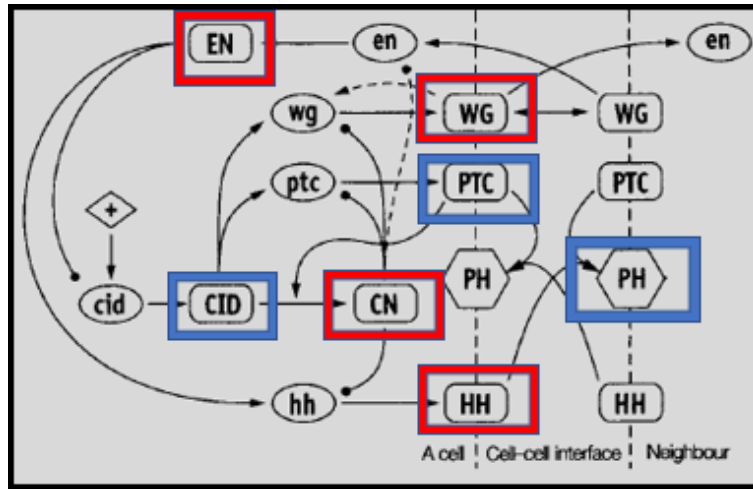


**Figure 1.2:** Robust segment-polarity gene network model; Seven protein components can be further analysed for simple analysis based on the protein production rates: *engrailed* (EN), *wingless* (WG), *cubitus interruptus* (CID), *hedgehog* (HH), *repressor fragment of CID* (CN), *patched complex* (PTC) and *patched-hedgehog complex* (PH); Simplification is based on the interactions between the components indicated by the arrows ; Modified from von Dassow *et al.* 2000

Epithelial tissue movements are necessary for the demarcating boundary of different adult body organs and segments in the organism (Guillot and Lecuit 2013). This flow of cells goes on to cover the anterior head region in a *Drosophila melanogaster* embryo simultaneously during the dorsal closure (Solon *et al.* 2009) stage when head involution actually begins (VanHook and Letsou 2008, Davies 2013). The sheet-like epithelial layer is composed of cells connected to each other at lateral junctions by cadherin and integrin class of proteins, and these are polarised along their apical-basal axes (St Johnston and Sanson 2011).

### 1.2.1 Relevancy of studying involution phenomenon

During *Drosophila* embryogenesis after the gastrulation process, the epidermal layer cells progress to spread towards the anterior pole of the embryo. The cells initially spread dorsally after which the entire tissue translocates. This progression has been noted to be not associated with any cellular protrusions, for example, lamellipodia or filopodia which indicates the absence of any active crawling. Such a sort of progression was studied by Czerniak *et al.* 2016, which leads to a positioning of segments along the Anterior-Posterior (A-P) axis in the embryo with equal width. Segment width was defined as the distance between the intersegmental grooves which cause indentations in the dorsal epidermis of the embryos during HI. Also during this process, the cells in the tissue rearrange themselves with periodic differences in the cells shapes at the parasegmental boundaries. The number of cells also remain fixed till HI is completed and hence the system can be considered closed.

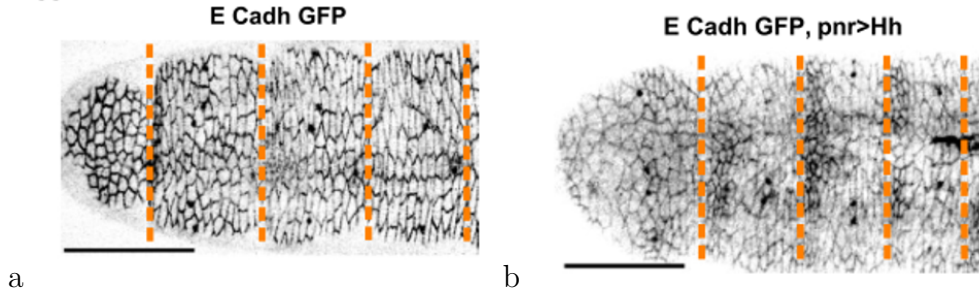


**Figure 1.3:** Segment width observation in embryos; Confocal images of E-cadherin-GFP tagged embryos of (a) WT and (b) overexpressed-Hh indicating equal and unequal segment widths marked by dashed lines; Scale bars = 50  $\mu m$ ; Reproduced from Czerniak *et al.* 2016

### 1.3 Genetic regulation of tissue mechanics at intrasegmental boundaries

The *Drosophila melanogaster* embryonic development involves a hierarchy of patterning from maternal gradients, through gap-gene expression and pair ruled genes. Such gradients result in an anterior to posterior compartmentalization in the embryo with segment polarity genes defining the boundary between the cells in the epithelial layer (Sanson 2001). At these parasegmental boundaries along with secretion of Hedgehog (Hh) and Wingless (Wg) proteins, even cell mechanics has been shown to be modulated (Czerniak *et al.* 2016) (Refer Fig. 1.3). Understanding the self-organizing principles which are controlling the underlying segment width control by modulations in the cellular shape pattern in such epithelial tissue spreading is necessary for identifying crucial factors in cell migration, tissue growth, and regeneration.

#### 1.3.1 Role of Hedgehog (Hh) signaling in segment positioning

Hedgehog (Hh) is an intracellular signaling molecule which has essential roles in segment development of the larval body. In a developing *Drosophila* embryo, when the body segments are forming, cells synthesizing the transcription factor engrailed also express Hedgehog. This Hh interacts with receptor protein Patched which in turn leads to cells with activated Hh-Patched synthesizing a different extracellular signaling molecule Wingless (Wg) (von Dassow *et al.* 2000). The effects of Wingless and Hedgehog on rows of cells in each segment of the *Drosophila* embryo establishes a positional code that results in noticeable anatomical features along the anterior-posterior axis of the segments (Ingham and McMahon 2001). The activation of the Hedgehog pathway leads to a decrease in E-cadherin and tight junctions through increase in Snail protein production thus giving the phenotype of relaxed cell boundaries (Li *et al.* 2006). Therefore, the Hh signaling coupled with the tissue biomechanics results in the self-organized distribution of the epithelial cells.

A description of the Hh-signaling pathway has been described in Fig. 1.2, where the robust segment polarity gene network has been modelled as a simple continuous dynamical model with the help of ordinary differential equations (ODEs). Steady-state solutions to these ODEs can reveal and quantify the transcription rates, binding rates and activation

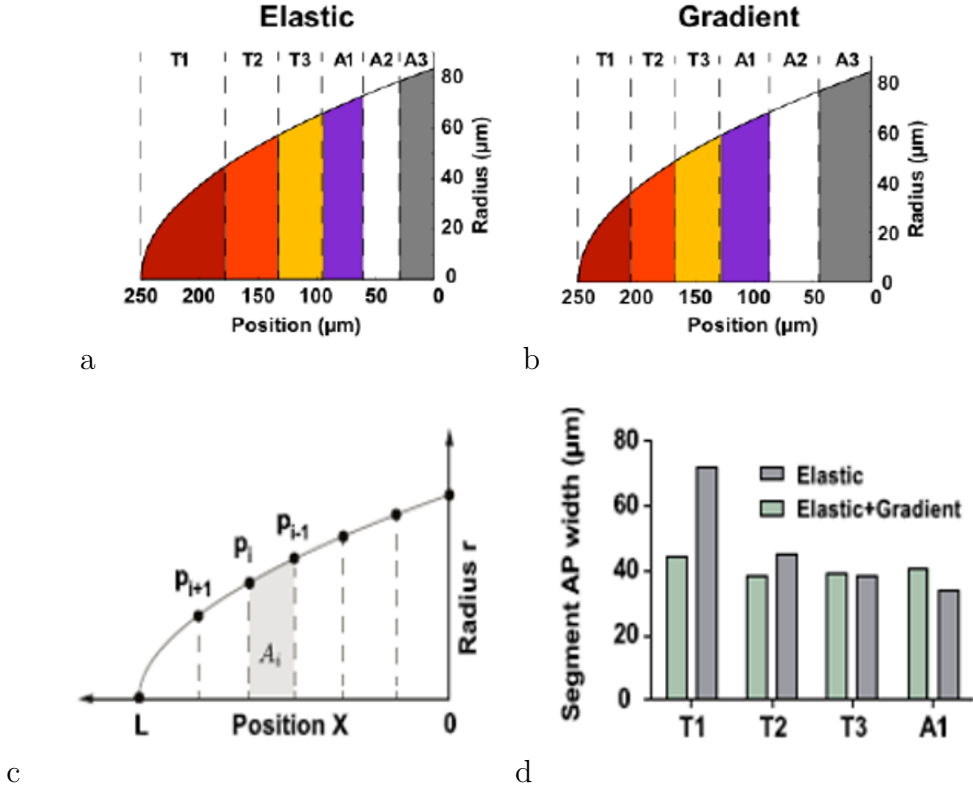


**Figure 1.4:** 1D Elastic epidermal sheet models; (a) represents the purely constant elastic model while (b) represents the gradient of active tension ( $f_t$ ) model; (c) gives a schematic of the nodal positions of the spring-like tension along the geometry of the embryo; (d) gives the data of segment-width control difference between the two models wherein equal width are observed for the gradient model and not for the elastic only model; Reproduced from Czerniak et al 2016

kinetics of the protein molecules involved in the complex process which can be further used in simulation setups.

## 1.4 1D Elastic epidermal sheet

Czerniak *et al.* 2016 proposes two theoretical models of embryonic tissue spreading mechanism in 1D to explain the periodic patterned junctional tensions at play (Refer Fig. 1.4). The 2D elastic epidermis was modeled on a description of the bulk and shear modulus where the patterned forces were summed along the circumferential and tangential directions and the force interactions between individual segments (represented by nodes) are calculated as force density ( $f_i$ ), acting on each node  $p_i$ , in Eqn. 1.1.

$$f_i = K((A_0 - A_{i-1}) - (A_0 - A_i))t_i \quad (1.1)$$

where the stiffness of sheet-like tissue material is denoted by 'K'; the area of the  $i$ th segment is given by  $A_i$  and the tangential vector at  $p_i$  which is normalized is denoted by  $t_i$ . Under equilibrium conditions, all the forces and the segmental width area as calculated analytically are balanced:

$$f_t(x(p_i)) + f_i = 0 \quad (1.2)$$

$$(A_i - A_{i-1}) = 0; \forall i = 2, 3, 4, 5, 6 \quad (1.3)$$

## 1.5 Understanding segment width and cell shapes during involution process

For this work, the motivation is to approach the problem using a Potts (Graner and Glazier 1992) simulation (Albert and Schwarz 2014) of 2D and 3D geometrical *Drosophila* tissue. The specific questions that are being investigated are

1. How are cell-shape patterns generated by modulating only cellular mechanics?
2. Whether the cell shape patterns in the tissue organization can be recapitulated by junctional tensions in the presence of a Hh gradient with the CPM model.
3. If both tissue biomechanics, as well as the biochemistry at the cellular level, is controlling segment width, then what is the nature of the coupling between the two? To understand the intricacies of feedback loop that may exist between the two and improvise that in our simulation model.

Although there are studies which have tried to explain such cell shape patterns using vertex model and convergent extensions, most of these have significantly minimal or no feedback terms from the genetic components (David *et al.* 2014). In this particular CPM model, the goal is to achieve an integrated model of biomechanics along with the biochemical coupling terms using a diffusion solver.

# Chapter 2

## Model

The elastic 1D epithelial sheet model has been adopted from [Czerniak \*et al.\* 2016](#) and used for 2D and 3D simulation study to recover the same segmentation of junctional boundaries observed in the wild-type variety of fruit fly embryos seen under the confocal microscope to show a better understanding of the forces controlling such type of self-organization. Along with the elastic model, it has also been hypothesized that a morphogen gradient of chemicals also controls the segment width which has been attempted in this study.

### 2.1 Elastic tissue simulation based on CPM formalism

For the Cellular Potts Model formalism, the energy of the cell is modeled on the mechanical properties of the cell as a whole. The CPM formalism, based on the energy minimization, allows us to integrate forces acting at mesoscopic scales into a predefined Hamiltonian. Generally speaking, the total energy of the system can be assumed to be composed of:

$$\mathbf{H}_{total} = E_{Contact} + E_{Volume} + E_{Chemotaxis} \quad (2.1)$$

In this particular elastic model, there is surface energy of the cell present instead of chemotactic energy.

$$\mathbf{H}_{total} = E_{Contact} + E_{Perimeter} + E_{Surface} \quad (2.2)$$

The constructed Hamiltonian in our case is defined as follows:

$$\mathbf{H} = \sum_{(i,j)} J_{(i,j)} (1 - \sigma_{\delta_i, \delta_j}) + \gamma_s (S_1 - S_2)^2 + \gamma_v (V_1 - V_2)^2 \quad (2.3)$$

where for 2Dimensional systems  $\gamma_s$  is a measure of cortical tension forces acting due to the elasticity of the cell,  $\gamma_v$  is a measure of the surface pressure on the system due to area conservation,  $S_2$  and  $V_2$  denote the target surface area and target volume of the cell object while  $S_1$  and  $V_1$  denote the instantaneous surface area and volume of the particular cell in the tissue for 3D. Again for 2D systems,  $S$  and  $V$  correspondingly convert to the perimeter and surface area of the cell instead of the surface area and volume.  $J$  is the contact energy which is the function describing the likeliness of cells to stick to each other;  $\sigma$  signifies interaction between particular cells;  $i, j$  indicates cell number.

The expression in 2D looks like:

$$\mathbf{H} = \sum_{(i,j)} J_{(i,j)}(1 - \sigma_{\delta_i, \delta_j}) + \gamma_s(P_1 - P_2)^2 + \gamma_v(S_1 - S_2)^2 \quad (2.4)$$

where P represents the perimeter of the cell with all other terms remaining the same.

The model uses a probability distribution of acceptable pixel changes to the system which is based on cellular automata.

$$\Delta H = H_{instantaneous} - H_{previous} \quad (2.5)$$

It is an exponential probability distribution where the two input parameters are the change in Hamiltonian, i.e., change in energy at each iteration step due to appearance and vanishing of pixels and the temperature at which the system is simulated at, which contributes to the stochastic nature of the simulation study.  $k_B$  is the Boltzmann constant taken to be equal to 1 according to computation necessities. All positive energy changes are favored ( $\Delta H > 0$ ) alongwith negative energy changes with probability of accepting the configurational change according to the eqn. 2.6.

$$p_{Acceptance}(Probability) = e^{\frac{-\Delta H}{k_B T}} \quad (2.6)$$

The Cellular Pott's Model utilizes Markov Chain Monte Carlo (MCMC) process and the Metropolis algorithm for the above descriptive phenomenon.

## 2.2 Effective model of morphogen diffusion

Hedgehog is not a freely moving protein molecule, and it only activates in a thin row of cells lying adjacent to the *Engrailed*-expressing cells in the epidermal tissue of a developing embryo, thus acting as a local paracrine factor. The primary criticism of using any robust segment polarity gene network of hedgehog pathway (von Dassow *et al.* 2000) to incorporate with the mechanical tension model lies in the kinetics of the transcription regulatory mechanisms of production of Hh and Wg which occurs much later in the developmental process of embryogenesis during wing formation. Hence it would be fruitful to choose an appropriate model of morphogen gradient at the intra-segmental boundaries which would be more likely to affect the dynamics during HI (Kicheva *et al.* 2007).

The thin row of cells with local Hh-activated Patched complex helps in transcription of some genes such as decapentaplegic (Dpp). Kicheva *et al.* 2007 have already shown how the kinetics of the morphogen gradient affect the range of the secreted morphogens like Decapentaplegic (Dpp) and Wingless (Wg) in a developing fly wing during embryogenesis (Fig. 2.1(b)). The aim is to reproduce such an intra-segmental morphogen gradient created due to the activity of Hh-induced Dpp and Wg production into the cellular pott's model which will affect the junctional tension. Kicheva *et al.* 2007 concluded that the positional spreading of morphogens is controlled by four vital governing factors: the effective diffusion coefficient, both the production and degradation rates, and the immobile fraction. By knowing which acts at a faster timescale: the morphogens or the tissue mechanics, can reveal about the dominating force in the segment width. The published values of the diffusion speeds of the morphogens with the kinetics of the mechanics of the tissue progression it was found to be of a comparable order of magnitude which justifies incorporating a similar reaction-diffusion model of intra-segmental morphogen gradient formation by secretion of junctional cells into the pott's model. The governing reaction-diffusion equation will look like:



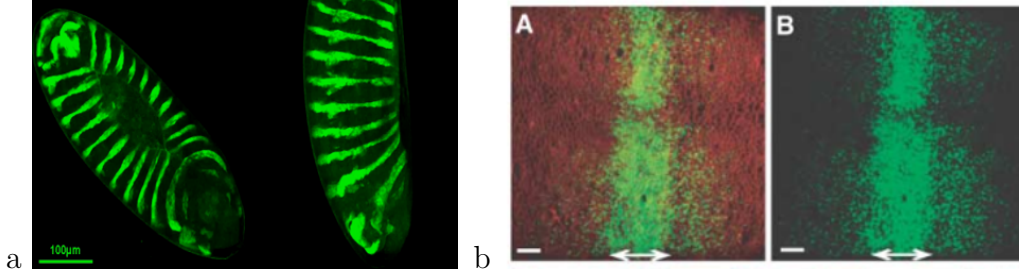


**Figure 2.1:** Epidermal spreading observed during HI; (a) Epidermal spreading is seen during HI along with zippering of amnioserosa indicating dorsal closure which leads to evenly spaced segments; (a) Taken from Czerniak *et al.* 2016 and (b) represents the wing disc of fly embryo with the endogenous source showing the expression of Dpp-tagged-GFP (marked with double arrow). Negative staining of the cells was done using a styryl dye [marked with red in (A)]. Scale bars, 10 mm; (b) Taken from Kicheva *et al.* 2007.

$$\frac{\partial[C]}{\partial t} = D \frac{\partial^2[C]}{\partial x^2} - k[C] + j_0 \delta(x) \quad (2.7)$$

Assuming a one-component reaction-diffusion system which can propagate spatially and temporally,  $C(x,t)$  is the concentration of the morphogen under question,  $D$  is the diffusion coefficient of  $C(x,t)$ ,  $k$  is the degradation constant of  $C(x,t)$  over time  $t$  while  $j_0$  is the source term with an additional  $\delta(x)$  spike. Commenting on this model,  $C(x,t)$  is the concentration of morphogen Dpp which as shown in Fig. 2.1(b) diminishes over a spatial dimension ( $x$ ) and over time ( $t$ ) which has been measured experimentally by fluorescence measurements in Kicheva *et al.* 2007.

For preliminary analysis a 1D morphogen gradient was studied using the above model system borrowed from Kicheva *et al.* 2007 to showcase the gradient without the steady-state solutions of the partial differential equation under fixed no-flux boundary conditions with initial conditions.

# Chapter 3

## Methods

For tissue simulations, the software CompuCell3D (Swat *et al.* 2012) has been used which is built upon the cell sorting algorithm of Cellular Potts Model. Softwares used for data analysis and processing of image data are MATLAB 2016a (The Mathworks Inc.), Enthought Canopy (Python platform), FIJI (ImageJ) (Schindelin *et al.* 2012), Packing Analyzer Version 2 (Aigouy *et al.* 2010) and Microsoft Excel.

### 3.1 Simulation Methods

#### 3.1.1 Pott's model in CompuCell3D platform

CompuCell3D (CC3D) (Swat *et al.* 2012) is an open-source simulation environment, compiled in C, which utilizes a cellular pott's approach to model cell behavior applied globally for multi-cell, single-cell based modeling of tissues, organs, and organisms (Andasari *et al.* 2012).

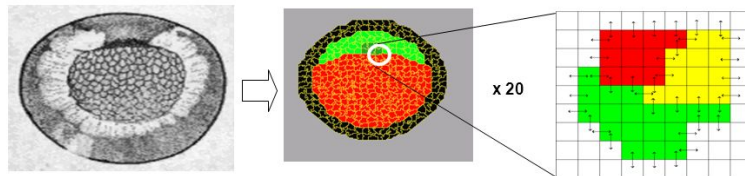


**Figure 3.1:** Working principle of Pott's model in CC3D; Image of a blastula or group of cells seen under the microscope is on the left; The group of cells can be represented by group of square cells (middle) in the computer simulation set-up marked by different colours; When zoomed into the simulation each cell is the sum of discrete pixels coloured differently; This schematic explains the principle of using cellular automata in the CPM model

An elliptical shape was created with fixed boundary value conditions to imitate the actual geometrical embryonic shape in Cell Draw. A parametric representation of an ellipse is

$$\frac{x^2}{a^2} + \frac{y^2}{b^2} = 1 \quad (3.1)$$

The file created by Cell Draw is known as a Potts Initialization File (or PIF) which is a matrix generated of alphanumeric values which can be interpreted as lattice values

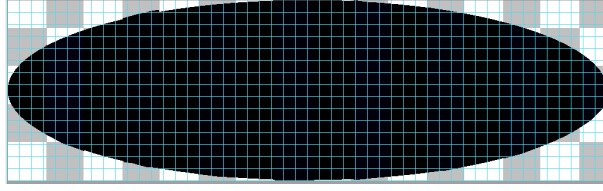


**Figure 3.2:** Fixed geometry of the model in CC3D; For initial conditions embryonic shape is modelled as an ellipse which is then filled with square cells of given pixel dimensions; Boundary conditions are fixed no-flux

in our domain-field. The lattice initialization file tells CompuCell3D how to lay out or assign the simulation lattice pixels to cells.

Control setups were carried out in 2D and 3D with changing boundary conditions, i.e., fixed or open or periodic, to imitate the 1D elastic model from Czerniak *et al.* 2016. Initially, the model has been used to produce a minimal description of the conditions necessary to reproduce experimental observations already described which serve as control calculations for following measurements involving perturbations to the system.

For simple and heuristic process, only a quarter of the elastic epithelial sheet was simulated later on with distinct segmentation boundaries. This was achieved by restraining boundary value conditions on Python and Cell Draw.

### 3.1.2 Observation of segment positioning by regulation of cortical tension ( $\gamma_s$ ) and surface tension( $\gamma_v$ ) parameters

A quarter of the elastic sheet model with proper boundary conditions in Fig.3.3 is initialized with different segments. Control calculations were done for a variable number of Monte Carlo steps for different values of parameters keeping the temperature of the system fixed at 40 a.u. Number of cells in each segment were also varied as well as held constant to see the effect on cell shapes as well segment positioning under equilibrium conditions.

#### Aspect Ratio Calculation

From Fig.1.4(a) and (b), it is observed that

Each segment width  $\approx 5$  cells approx.

Each cell size of cells along equator  $\approx \frac{50}{5} = 10$  microns

Total number of cells in one quarter/half along equator of the embryo =  $\frac{250}{10}$   
= 25 cells approx.

Aspect Ratio =  $\frac{Width}{Height} = \frac{250}{80} = 3$  approx.

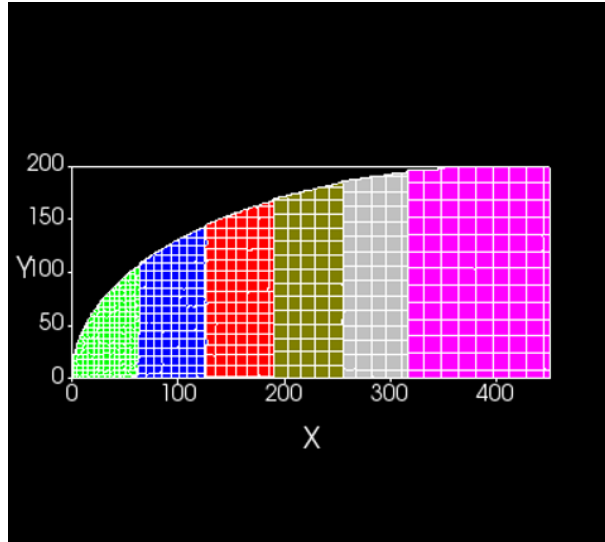


**Figure 3.3:** Simulation geometry with six segments; Initial condition of elastic sheet model with six segmentation boundaries with approximately equal number of cells in each segment

Variable	Value (a.u.)	Range	Reported Values (a.u.)	References
Temperature (T)	10-40		50	Belmonte <i>et al.</i> 2016
$n_{orders}$ (neighbour order)	2,4		2,4	Belmonte <i>et al.</i> 2016
Surface tension coefficient ( $\gamma_v$ )	0.005-4.0		1000	Magno <i>et al.</i> 2015
Cortical tension coefficient ( $\gamma_s$ )	0.01-4.0		5	Belmonte <i>et al.</i> 2016
Contact Energy (Cell-Medium) ( $J_{Cell-Medium}$ )	10-100		10	Belmonte <i>et al.</i> 2016
Contact Energy (Cell-Cell) ( $J_{Cell-Cell}$ )	10-100		10	Belmonte <i>et al.</i> 2016
Monte Carlo Steps (MCS)	10000-400000		This study	
Boundary Value Conditions	Fixed (Elliptical) Periodic (Square)			

**Table 3.1:** Comparison of different parameter values between simulation and experimental study (a.u. - arbitrary units)

### 3.1.3 Measures of cell shapes

For analyzing shapes of the cells in the tissue simulations as well as experiments, two measures were used: 1) Circularity and 2) Eccentricity. The circularity of a cell was defined as

$$Circularity_{Cell} = 4\pi \times \frac{Area_{Cell}}{Perimeter_{Cell}^2} \quad (3.2)$$

It is a measure of how much a given shape deviates from an ideal circle. The eccentricity of a cell was defined as

$$Eccentricity_{Cell} = \frac{MajorAxis_{Cell}}{MinorAxis_{Cell}} \quad (3.3)$$

The perimeter is calculated by summing up the outlying lengths of the discrete pixels lying at the boundary which constitutes the cell while the area is calculated by summing the area of the of the pixels which form one particular cell.

### 3.1.4 Voronoi tessellation using delaunay algorithm

From the tissue simulations, centroid values of each cell in the tissue were extracted for every iteration point or Monte Carlo Step (taken to be an analog of time here). The Center of Mass were calculated using the centroid values which were generated using a CC3D plugin. This plugin monitors changes in the lattice and updates centroids of the cell regardless of boundary value conditions (periodic or fixed):

$$X_{COM} = \Sigma_i x_i; Y_{COM} = \Sigma_i y_i; Z_{COM} = \Sigma_i z_i \quad (3.4)$$

Where i denotes pixels belonging to a given cell. The centroid values were divided by the cell volume to obtain coordinates of a center of mass.

$$X'_{COM} = \frac{X_{COM}}{V}; Y'_{COM} = \frac{Y_{COM}}{V}; Z'_{COM} = \frac{Z_{COM}}{V} \quad (3.5)$$

These center of mass values were then called into a Python script (courtesy of Neha Khetan, SOCM Lab 2017) which uses a Delaunay triangulation algorithm and produces a Voronoi tessellated image of the initial and final time points of the simulation. The algorithm uses an empty circumcircle criterion where for a set of points in a 2D field, a Delaunay triangulation of these points calculates the circumcircle associated with each triangle of points, so that contains no other point in its interior (Okabe *et al.* 2008).

### 3.1.5 Reaction-Diffusion solvers

A simple 1D reaction-diffusion model is implemented in MATLAB using the **pdepe** solver according to the eqn. 2.7 and the concentration of the morphogen is plotted over time and space. The boundary conditions are fixed in 1D with no-flux conditions and the initial conditions for  $t = 0$  is a function of position (x).

For simulating cells secreting morphogen and creating morphogen gradient over space and time, an inbuilt reaction-diffusion solver in CC3D was made use of.

Parameter	Simulation Value	Reported Values	References
D (Diffusion coefficient)	$10^{-6}$ a.u.	$0.1 \pm 0.05 \mu m^2/s$	Kicheva <i>et al.</i> 2007
k (degradation constant)	$2.5 \times 10^{-4}$ a.u.	$2.52 \times 10^{-4} \pm 1.29 \times 10^{-4}/s$	Kicheva <i>et al.</i> 2007
$j_0$ (source term)	4 a.u.	$3.98 \pm 2.34$ molecules/ $(\mu m \times s)$	Kicheva <i>et al.</i> 2007

**Table 3.2:** Variable parameters comparing simulation and experimental data for the morphogen diffusion study using Dpp-tagged-GFP

## 3.2 Experimental Methods

### 3.2.1 *Drosophila* embryo preparation and microscopy

For the wild-type set of experiments, the *Drosophila* strain used was: *en-DE-cadh-GFP* (E-cadh-GFP) (from Yang Hong Lab, University of Pittsburg, USA) which expresses GFP with the engrailed promoter. Activation of the engrailed gene in the cells express the Hedgehog protein. For the set of experiments with the overexpression of the Hh gene, the *Drosophila* strains used were: *Ubi-DE-cadh-GFP/CyO;pnr-Gal4/TM6B* and *UAS-hh* (a gift from N. Perrimon, Harvard Medical School). Males flies from *UAS-hh* and females flies from *Ubi-DE-cadh-GFP/CyO;pnr-Gal4/TM6B* flies were used to generate germline clones for the observing the variation in junctional tension in the epithelial layer and thus the distribution of the tissue.

The driver *pnr-GAL4* was explicitly used to affect the different signaling pathways in the dorsal epidermis during a late stage of the developmental process. Pannier does not affect earlier stages of embryogenesis associated with segmentation since it is expressed late in development. Under this driver, expression of a dominant negative form of the EGF receptor (UAS-EGFR-DN) or abnormal positioning of wingless (UAS-Wg) fails to show any phenotype.

Embryos were collected at 25°C, aged for 16-18h at 18°C and then dechorionated in 50% bleach for 1:30 min, washed with water, and mounted on a glass bottom microwell dish. The dish had been previously coated with heptane glue. Mounted embryos were then covered with halocarbon oil and imaged at room temperature. The procedure has been adapted from Czerniak *et al.* 2016 with minor changes.

All the images were obtained using confocal microscopy. The two crucial points to remember before imaging were; first, the embryos should be at the correct stage of development when the HI of the anterior head region is observed. Secondly, removal of the chorion, the protective shell of the embryo, before imaging. The chorion is reflective, and thus compromises image quality if not removed. The dorsal and lateral views of the embryos were generated with a Dragonfly spinning disk head on an inverted microscope (Andor) and a Yokogawa CSU-X1 spinning disk head on an inverted microscope (Olympus) [oil immersion lens] at 60X and 40X with 2 and 3 min time resolution at room temperature (25°C). Negligible drift was observed in the stage under temperature and pressure stabilizer control.

### 3.2.2 Image processing

All the time-lapses were analyzed using FIJI, Matlab, and Packing Analyzer v2. The apical cell surface area and perimeters were measured on embryos expressing E-cadh-GFP-tagged by semi-automatic segmentation of sum and maximum projections using Fiji and Packing Analyzer. The images were then converted into black and white binary format; background light was subtracted and used for calculating the intensity of pixel values. And the center of mass of cells was determined afterward.

For measuring tissue progression speeds, Manual Tracking feature of Fiji and the MOSAIC (Sbalzarini and Koumoutsakos 2005) plugin tool was used.

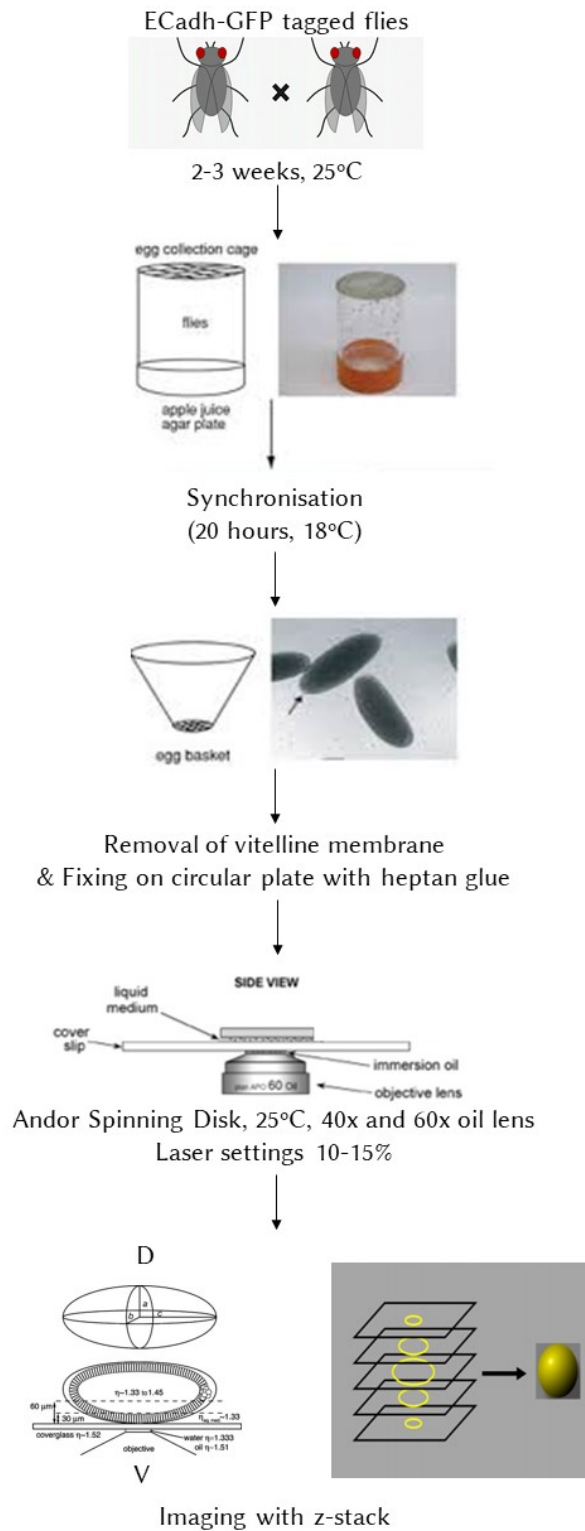


**Figure 3.4:** Experimental protocol flowchart followed for imaging the flies using confocal microscopy along z-stack (D - Dorsal; V - Ventral)

# Chapter 4

## Results

The results are in two different parts, firstly, the image analysis of microscopy data from performed experiments and secondly, the simulation results and the analysis of the 2D and 3D model with emphasis on the equal segment width pattern.

### 4.1 Experimental Results

As described in Sec. 3.2, observation of the HI process was done using confocal microscopy of the wild-type as well as the embryos in which Hh was overexpressed. Time-lapse microscopy movies were analyzed to validate the tissue movements while HI is occurring. When HI is completed, a time-point is fixed, and the tissue structure is observed using segmentation methods with differences in cell shapes and equal segment width distinctly noticeable.

#### 4.1.1 Progression of epithelial tissue during head involution

The progression of epithelial tissue at the anterior pole of the embryo was imaged, both laterally and dorsally. The time course of progression of the tissue was measured, and the calculated velocity of movement of the tissue segments using denticle tracking was found to be comparable to the laser ablation measurements reported by Czerniak *et al.* 2016.

After tagging the denticles in Fig. 4.1, for analysis, only denticles which showed tracks for more than 90 % of the frames were chosen to avoid misrepresentation. The final tracks were plotted along X and Y directions, and the Euclidean distances traveled were calculated as in Fig. 4.2. The tracks show deviations along X and Y axes with a noticeable rotating movement due to the progression of the tissue along the elliptical boundary of the embryo.

The cumulative distance progression over time and the time-averaged velocity plots shown in Fig. 4.2 report speed values of 0.02 - 0.05  $\mu\text{m}/\text{s}$  which is comparable with previously published results in Czerniak et al 2016 albeit using a different approach of measuring the progression velocities of individual segments (T1,T2,T3,A1,A2 and A3) in the tissue. Afterward by performing microsurgery using laser ablation the published linear velocity of progression was found to be approximately 0.3 $\mu\text{m}/\text{min}$ .



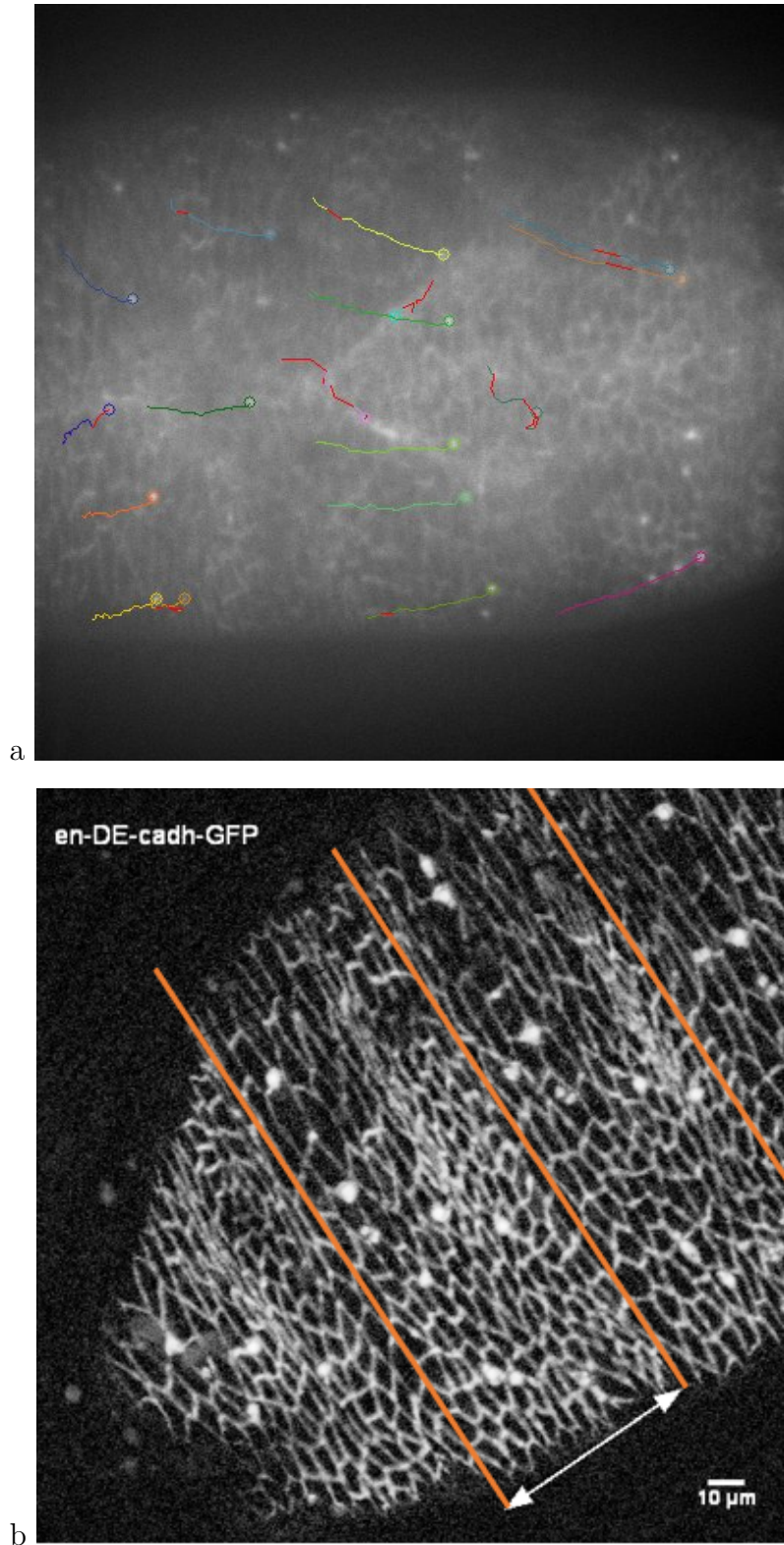


**Figure 4.1:** Particle tracking of denticles indicated by intense fluorescent points give an estimate of tissue spread velocity (a) Time lapse snapshot showing epidermal spreading in an embryo expressing *Ecadh-GFP pnr-GAL4 UAS-hh* with coloured lines showing the denticle tracks; (b) Time stamp snapshot showing the tissue organization when HI is just completed in an *en-DE-cadh-GFP* expressing embryo where each segment is highlighted by the double-sided arrow and demarcated by orange lines; Bright fluorescent spots indicate the denticles.

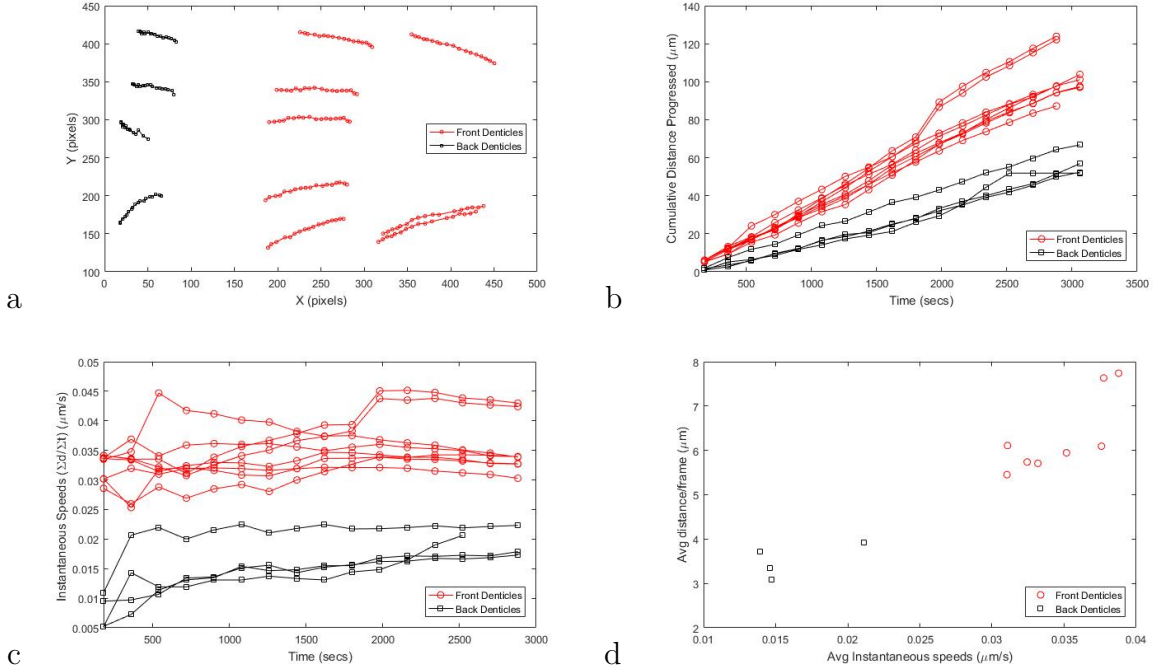


**Figure 4.2:** Analysis of the tracks of the denticles showed differences in movement of tissue based on positional configuration (a) Based on the direction of movement along A-P axis all tracks above 150 px along X axis are classified as Front Denticles (Red) and the rest as Back Denticles (Black); (b) shows cumulative distance progressed by the denticles over time; (c) represents the plot of instantaneous speeds of the denticles which shows a differential tissue movement over space, (d) plots the time-averaged distance cover by each denticle over instantaneous speeds

#### 4.1.2 Tissue segmentation after completion of HI

The progression of the epithelial tissue over the time course of the whole (HI) process which occurs around 12-14 hours under room temperature after fertilization and laying of the eggs was imaged for 1-3 hours by the method explained in Sec. 3.2. During this process after individual segments have fused due to zippering action during dorsal closure (Solon *et al.* 2009, VanHook and Letsou 2008), lateral progression appears almost linear along the anterior-posterior axis. When the leading edge, defined by the time  $t=0$  min when the epidermal tissue is at  $50 \mu\text{m}$  from the anterior pole of the head, fully covers the head region, the cells in the tissue rearrange themselves accordingly. This particular distribution of cells is caused due to the mechanical actomyosin forces acting inside the cells and cellular packing of the cells along with a gradient of Hh and Wg at the parasegment boundaries. One such final time-point when HI is completed in the wild-type embryo (*en-DE-cadh-GFP* (E-cadh-GFP)) is taken, and a portion of the tissue is analyzed in Fig. 4.3.

Observation of the cell shapes with the circularity measure defined previously in Sec. 3.1.3 revealed a periodic repetition band of roundish and elongated cells within each segment. This corresponded with high and low circularity measurements of cells wherein the circularity of roundish cells was around 0.7 and the circularity of the elongated cells was in between 0.1-0.2 (Refer Fig. 4.3(b)).

Heatmaps were plotted denoting the segmented cell center of masses showing posi-

tional variation in the area and perimeter of the individual cells in each segment of the epithelial tissue due to the differential forces at play. The preliminary data in Fig. 4.3(c) shows consistency with previously published data of regular pattern of area variation but still needs to be cross-checked with more sample data (embryos).

Voronoi tessellation was performed after extracting the cell center of mass (Fig. 4.3(d)) and the resulting graph, when overlapped on top of the original cell outlines, showed differences in the cell outlines or perimeters. This difference in cell shapes needs to be quantified using the coefficient of variation measure and polygonal distributions which may lead to answering questions about inherent anisotropies in forces which shape tissue morphogenesis.

In Fig. 4.4, packing analysis of the segmented tissue was performed wherein the polygonal approximation of the cells revealed the distribution of shapes to be skewed towards pentagonal (colored in yellow) and hexagonal (colored in grey) shapes (Fig. 4.4(b)) with mean value = 5.3 (Fig. 4.4(d)). The elongation tensor of the cells was also plotted along the X-Y axis (Fig. 5.2(a)(c)). It revealed a periodic repetition of a broader band of more elongated and narrow band of less elongated cells in each segment over space.

### 4.1.3 Unequal segment width in overexpressed-Hh embryos

In the second set of experiments with overexpressed-Hh, phenotypic change of more relaxed cell boundaries with roundish cells are visible all over the head region. The segment width was also found to be unequal as opposed to the WT case. This correlates with the published data in Czerniak *et al.* 2016 (Fig. 1.3). Similar tissue segmentation as in the case of WT embryos will reveal the differences in polygonal shape approximation with a different number of vertices and circularity measurements.

## 4.2 Simulation Results

Based on the experimental data of the tissue structure obtained from the wild-type and Hh-overexpressed embryos during the HI process, the goal first was to approach an agent-based CPM model with proper geometrical parameters to mimic the embryo system with looking at the mechanical aspect separately from the biochemical aspect and finally incorporate them both later on. Only the mechanical aspect has been studied in detail in this particular report.

### 4.2.1 Effect of differential adhesion energy between cell-cell junctions

Firstly, effects of the individual terms in Eqn.2.4 are investigated. The first term called the contact energy as described in Sec. 2.1 deals with differential cell-cell adhesion energy. The Differential Adhesion Hypothesis (DAH) states that the cells with similar contact energy values indicated by  $J$  would like to fuse or clump together. Thus DAH plays a determining role in the migration of cells according to favorable energy configuration. This is precisely shown in Fig.4.5 where green colored cells have lower contact energy values than blue colored cells. Thus the system prefers to sort in a manner in which green cells are closer to each other than blue cells.

Hence to negate the effects of the DAH all cells were assumed to have equal contact energy values in the system as shown in Fig.4.6. The medium was frozen to negate the

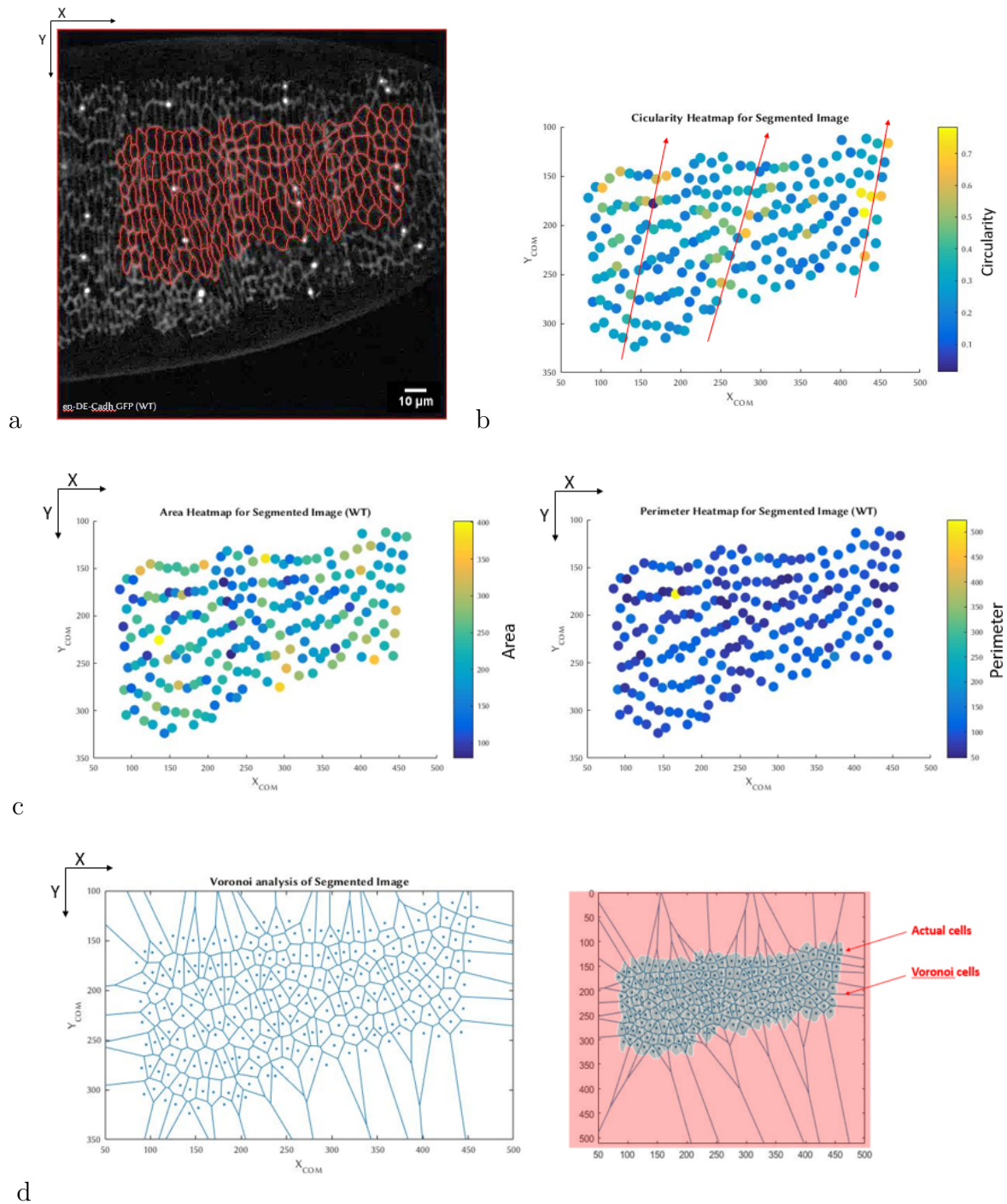


**Figure 4.3:** (a) Confocal time-stamp of WT *en-DE-cadh-GFP* tagged embryos after completion of HI with the red lines showing the segmented portion for analysis; (b) represents the heatmap of circularity of cells with a spatial periodic pattern observed; (c) plots the heatmap of cells according to the area (Left) and perimeter of cells (Right); (d) analyses the differences between the Voronoi tessellation of cells with the actual cell outlines

effects of interaction of cells with the medium and the boundary value conditions were initially taken to be rectangular/square periodic conditions. The system was iterated for 500 and 1000 MCS respectively, and no migration of cells was noticed thus validating that the DAH works.

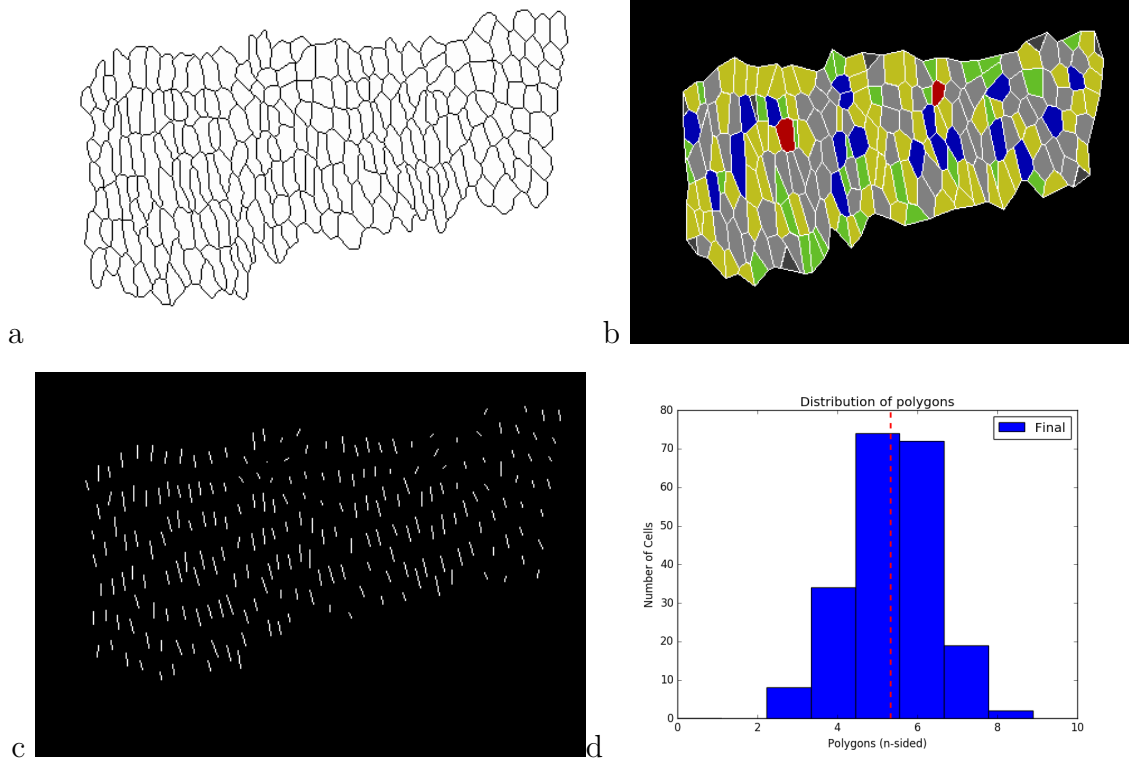


**Figure 4.4:** Polygonal approximation of tissue cells from experimental data (WT embryos) (a) shows the segmented portion of the cells; (b) gives a distribution of approximate polygonal cell shapes observed in the tissue with pentagonal (yellow coloured) and hexagonal (grey coloured) cells being more in number; (c) shows a regular pattern of elongated and non-elongated cells over spatial dimension by plotting the elongation tensor calculated from each of the cells; (d) Distribution of approximated regular sided polygon shapes in the segmented tissue shows bell curve around pentagonal and hexagonal shapes; *Dashed red line indicates mean  $n$ -side value = 5.3.*

## 4.2.2 Effect of embryonic geometry on tissue cell shapes

For the control setup for reproducing an earlier model of constant elasticity in Fig.1.4, fixed no flux elliptical boundary value conditions were imposed where the area of interest was filled with identical cells made up of square pixels of given dimensions. The cell size was varied from 10x10 pixels, 25x25 pixels to 50x50 pixels to match the aspect ratio of the actual embryo used in experiments.

For the embryonic model aspect ratio of elliptical geometry was tallied with the aspect ratio of the embryo as calculated in Sec. 3.1.2. It is also important to know for how many iterations, the system should be simulated for since higher number of Monte Carlo Steps requires higher computation power hence increasing runtime which is unfeasible. Thus circularity and eccentricity values of the whole system were plotted to observe that the system attains a steady-state circularity value following which the number of MCS were either chosen to be 500 or 1000 for further clarification (Fig.4.7).

A large system was created with each cell 50x50 pxs and an embryo of dimensions 400x200 elliptical shape with fixed boundary conditions on a frozen medium. The temperature value was fixed at 20, and the system was allowed to evolve to 500 Monte Carlo Steps. This is shown in Fig.4.8. From the simulation study of the larger cell system, the

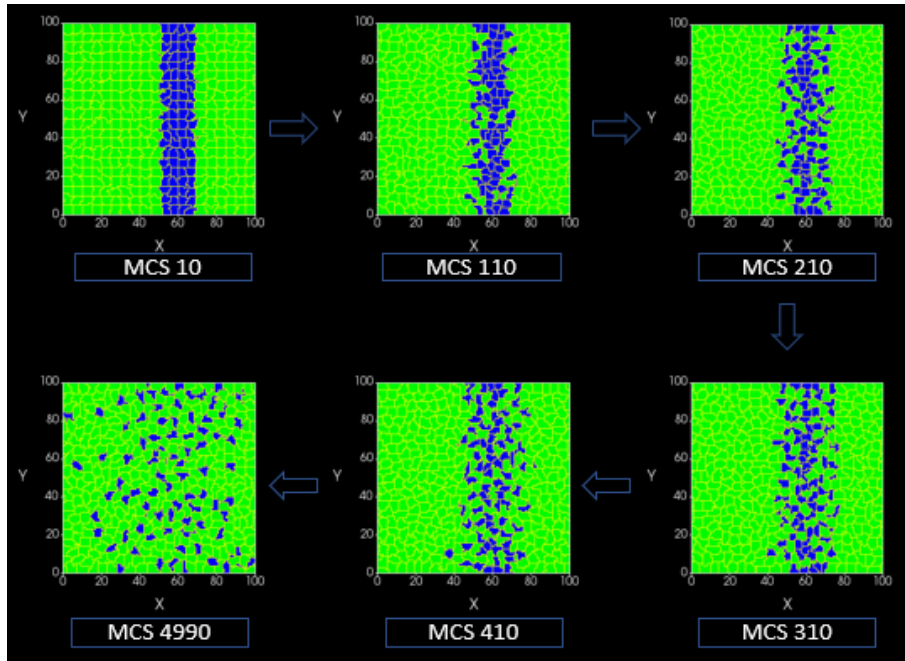


**Figure 4.5:** The above simulation shows the effect of Differential contact energy values in the migration of cells to a favourable energy state wherein blue cells like to stay away from other blue cells and moves away over time ( $J_{Blue-Green} < J_{Blue-Blue}$ )

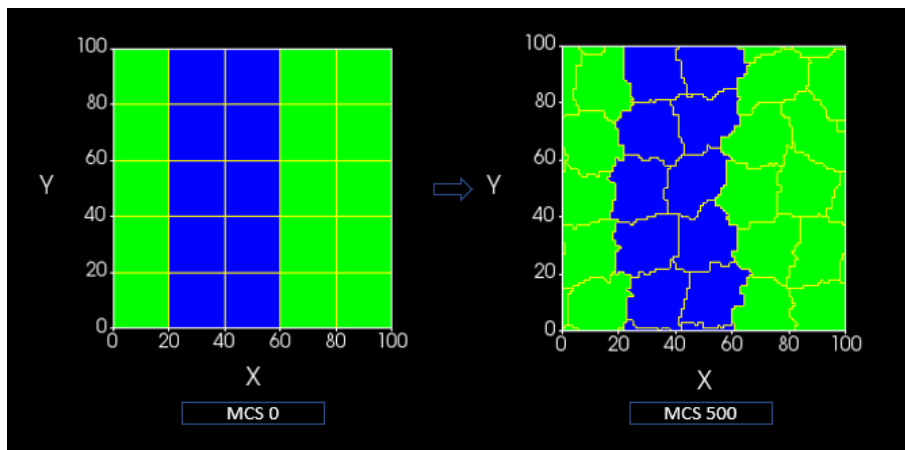


**Figure 4.6:** A square system of 100x100 was initialized filled with cells of 20x20 pxs where the shape change was observed after running it through the CPM algorithm; Shown for 500 MCS

center of mass of cells of the tissue was extracted, and the Voronoi analysis (Fig.4.9) was done which showed that the general tendency of cells in the tissue was to move from initial squarish cells to more hexagonal cells. The mean value of the polygonal shape was  $5.8 \approx 6$ . Also, cells at the periphery showed more deformation than the cells in the middle of the tissue. This was confirmed when the circularity values of cell in the tissues were plotted over the center of mass of the cells indicating positional as well as shape measures in Fig. 4.9(c)(d).

In a realistic embryo cell sizes are much smaller than the dimensions assumed above (50x50 pxs). To mimic a natural system, cell sizes were decreased to 25x25 pxs in a

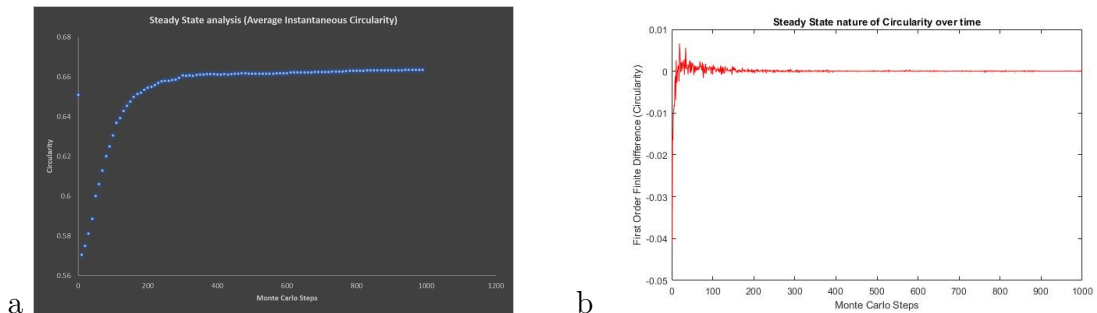
field of 500x200 domain and iterated for 1000 MCS at temperature value of 20. But the quantitative description remained the same where more irregular and non-circular cell shapes were observed at the periphery rather than in the middle of the embryo just due to the geometrical constraint of the system with fixed boundary conditions. This is evident from the Voronoi analysis in Fig.4.10 as well as the Heat Map of circularity over positional data of cells in Fig.4.10(c). These irregular shapes at the periphery may also be interpreted as artifacts of the system due to edge effects and needs to be looked into for larger systems.

Fig. 4.10 gives a visual as well as a quantitative description of translation of cell shape change from initial squarish to final hexagonal cells.

### 4.2.3 Interplay of cortical and surface tension regulates cell shapes

Cortical tension due to the actomyosin meshwork which generates contractility within individual segments of the epidermal tissue results in the formation of a gradient of tension. This cortical tension is represented by the perimeter and surface energy terms in the eqn. 2.4. The perimeter term incorporates the energy at the cell edges and boundaries with the coefficient  $\gamma_s$  indicating an absolute measure of the cortical tension. Theoretically, the surface term is less dependent on the cortical tension since the actomyosin mesh is mostly present at the cell boundaries. The surface tension coefficient  $\gamma_v$  represents the tension due to the cell surface receptors responsible for area conservation of cells.

For the next set of simulations, the system was chosen appropriately to be only the quarter of the head of the embryo, explicitly the six segments of T1, T2, T3, A1, A2 and A3, where HI is visible. Six different were made, excluding the last segment on the right in Fig. 4.11(b) and the system were initialized with equal cell density in each of the segments. Initial square cell sizes were 20x20 pixels, and the system was iterated for 1000 MCS. Initially, the contractility of the green and blue cells ( $\gamma_s$ ), keeping all other parameters controlled, were same which resulted in similar shapes across the system. The segment widths were also initialized to be equally marked by a band of green and blue cells. But making the  $\gamma_s$  of blue cells higher than the green cells resulted in the shape change of the blue cells and giving a pattern of roundish and elongated cells along the



**Figure 4.7:** Choice of iterating for fixed number of MCS depending on steady state nature of circularity; (a) shows the approach of steady-state of circularity after  $\approx$  300-400 iterations (depending on temperature of the system); (b) verifies the steady-state by calculating the difference of circularity at the iteration step and plotting the corresponding non-oscillatory graph

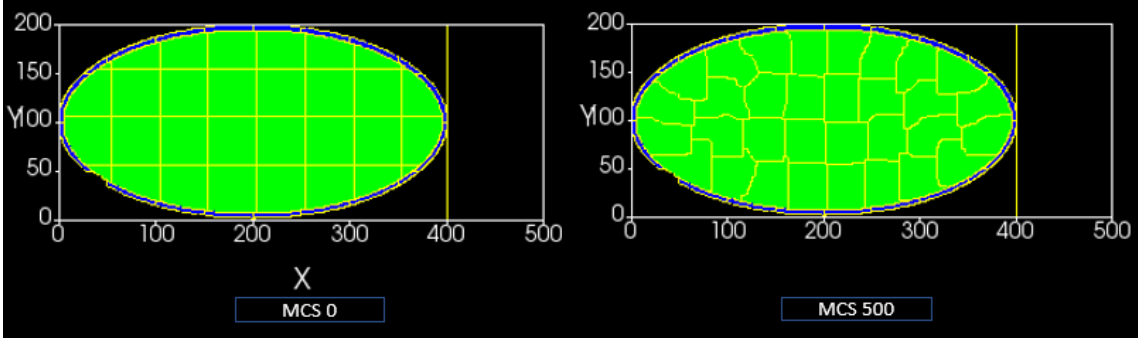


**Figure 4.8:** Elliptical fixed boundary conditions filled with cells of 50x50 pxs were simulated for 500 MCS at  $T=10$ ; Deformation of cell shapes were observed at the end of the simulation which were quantified by circularity data

X-axis which in this case is the A-P axis. The  $\gamma_s$  values also need to be in the same order of magnitude as the  $\gamma_v$  (surface tension coefficient) values for the change to occur otherwise the system will disintegrate towards a surface dominant energy flow. In such cases, the cells may merge to equilibrate the system according to the target surface area driven term. In these simulations, not very surprisingly, no change in segment width was observable, and the segments had equal segment width after the compiler runtime. Although uninteresting, this result reaffirms that the interplay of the cortical tension and the surface tension playing a role in the cell shapes of the tissue. And thus it allows us to explore with a gradient of contractility over space along the A-P axis.

#### 4.2.4 Recapitulation of overexpressed-Hh data in simulation setup

A simulation with six different bands of cells was initialized at  $T = 40$  units with square cells. Instead of starting with equal cell density as seen in the previous case in Sec. 4.2.3, the cell number is kept approximately constant in each of the individual segments. The cells nearer the anterior side of the head region are initialized to be made of smaller pixels than the one towards the posterior side of the A-P axis. All the parameters are kept controlled as shown in Fig. 4.12(c) with  $\gamma_s = \gamma_v = 0.1$ . Thus equal contractility value across the epithelial tissue results in broadening of the segments nearer to the head tip (Fig. 4.12(b)) and is purely based on the elastic properties of the cells the bands or segments arrange themselves unequally as predicted by the 1D analytical model shown in Fig. 1.4(a). It also recapitulates the pattern of segment width observed in embryos with overexpressed-Hh. Thus, this result serves as null hypothesis validation wherein we can predict that a gradient of contractility over space in each segment can recover the reported periodic contractile pattern of cell shapes and equal width during HI process in WT embryos.

#### 4.2.5 Organisation of tissue segments using bands of a contractile ring of cells

To recreate and understand the effects of a contractile band of cells on segment positioning and cell shapes a thin one row of blue cells were allowed to distinguish between broader equal segments of green and red cells. The cell number in the green and red segments are equal. Then starting from a case where all the parameter values are controlled, the  $\gamma_s$



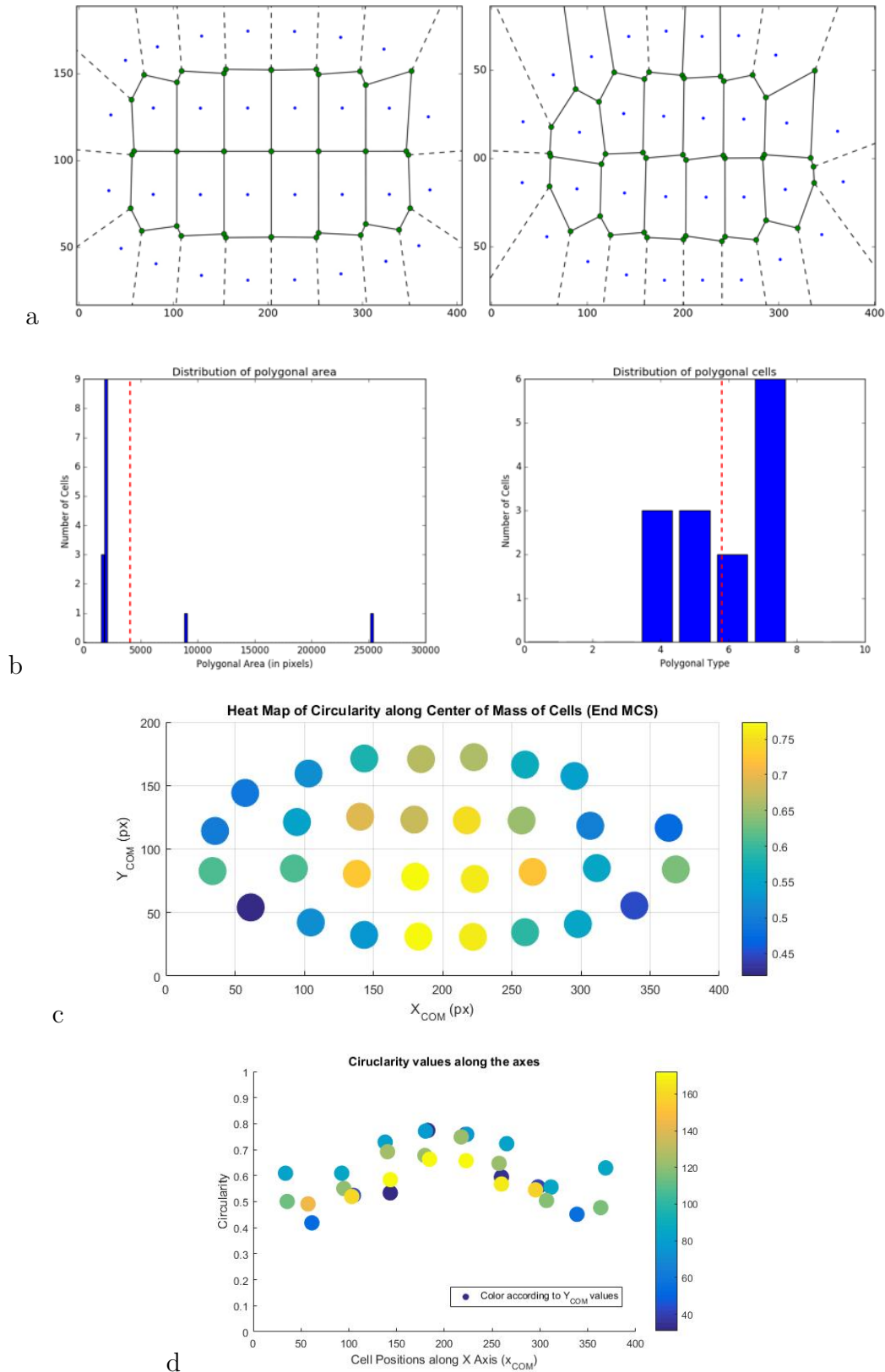


**Figure 4.9:** Simulation setup with fixed geometrical boundaries filled with large cells; (a) Voronoi tessellated image of larger cell system at Initial MCS 10 (Left) and final output at MCS 490 (Right); (b) Polygonal distribution of the final Voronoi output showing higher frequency of pentagonal and hexagonal cells; Dashed red lines indicate mean values; (c) Circularity of cells in tissue plotted as heat-map with cell COM data; (d) Circularity values plotted along X-axis while coloured with  $Y_{COM}$  values

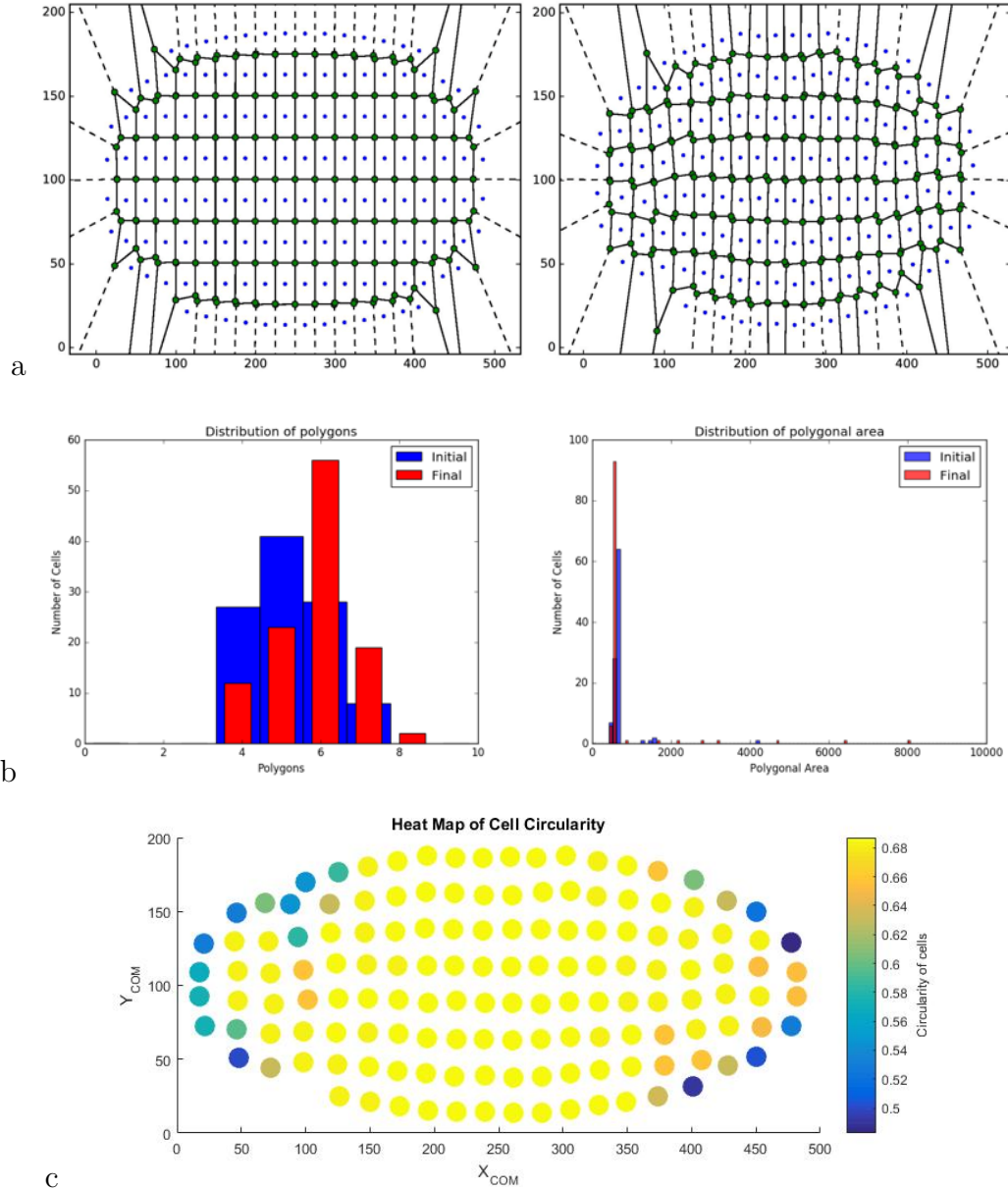


**Figure 4.10:** Simulation setup with fixed geometrical boundaries filled with small cells; (a) Voronoi analysis of larger elliptical system with smaller cells of size 25x25 pxs showing initial configuration (Left) and final output (Right); (b) (Left) Polygonal distribution of initial and final outputs present a trend of cell shapes to shift from square to hexagonal shapes while the polygonal area (Right) of the cells also distributes accordingly; (c) Circularity heatmap for larger system with smaller cells

value of the blue cells are increased in each setup to mimic the highly contractile nature of the blue cells which lie at the segmental boundary junctions.

As explained in Fig. 4.13, initially the system translates towards the right due to the arrangement of towards a configuration of equilibration of the cell area. With a periodic increase in contractility or cortical tension of the blue cells, the perimeter term of the Hamiltonian plays a dominant role, and the system thus tries to arrange itself for equal segment width due to a movement towards favorable perimeter configuration. This scenario resembles the movement of a system of three springs, along with an elliptical

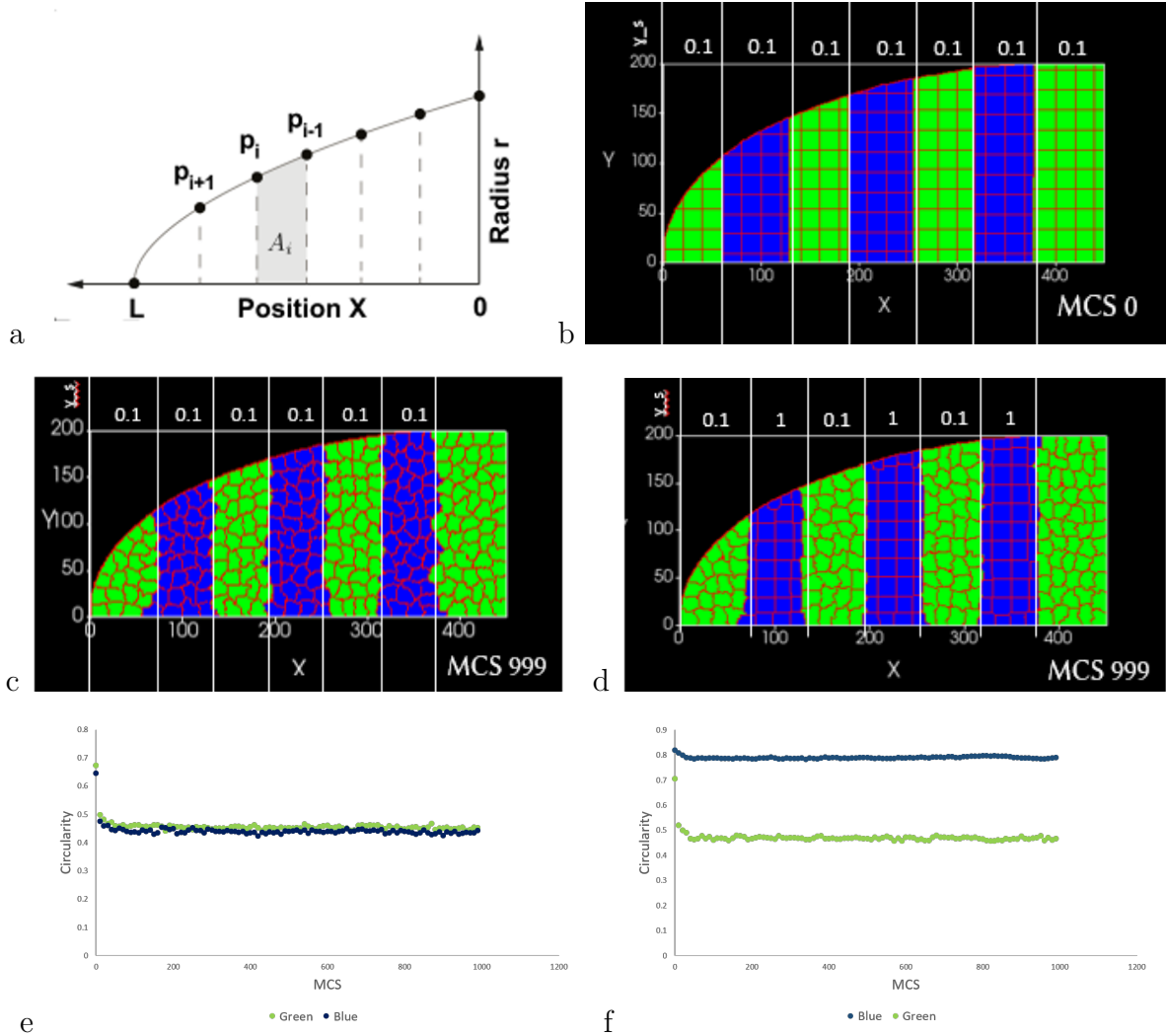
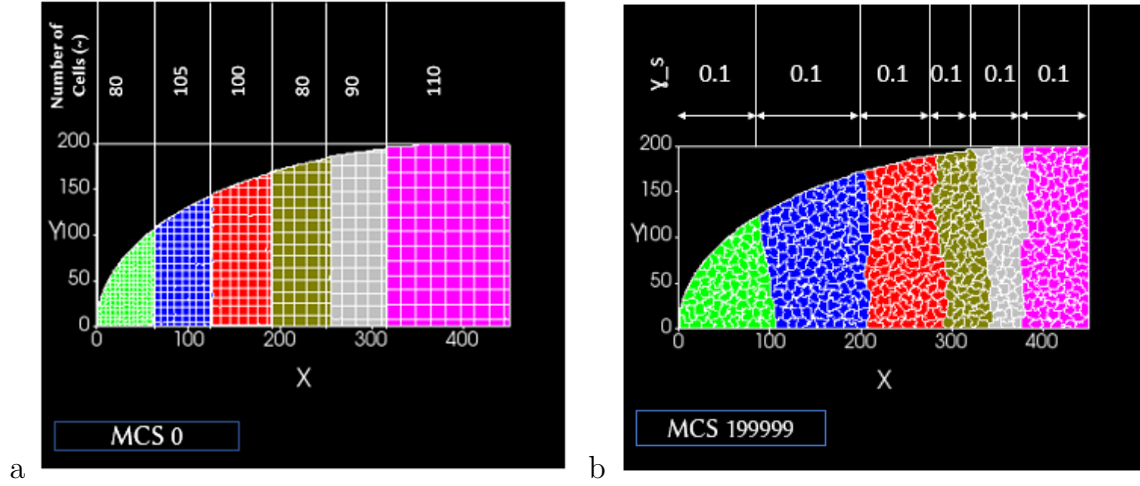


**Figure 4.11:** Regulation of cortical tension in cell shape analysis; (a) Schematic of segment nodes reproduced from Czerniak *et al.* 2016; (b) is the initial condition of the simulation setup with equal cell density in all the segments; (c) under same or equal contractility of all cells segment width remains unchanged with similar cellular shapes; (d) alternative bands of highly contractile cells output different cell shapes without any change in width; (e) and (f) reports the circularity values of the cells in the above simulations for (c) and (d) respectively

boundary, fixed at two ends and allowed to oscillate and reach a steady state position. This sort of arrangement over six individual segments is predicted to recover and validate the WT experimental data on segment width and cell shapes.

### 4.3 Incorporation of morphogen gradient

After the completion of the model with the elasticity and gradient of tension, a biochemical feedback loop needs to be incorporated into the contractility measure. Separately, a reaction-diffusion model of morphogen gradient has been employed to mimic the intra-segmental boundary pattern caused by Dpp and Wg expression at the parasegmental



Contact Energy Between		Value (Description) (Energy units)
Medium-Any Cell Type		0 (Medium Frozen)
Cell Type A – Cell Type A		10
Cell Type A – Cell Type B		50
Cell Type	Target Area	$\gamma_v$
Medium	None	None
Cell (Any Color)	25	0.1
Cell Type	Target Perimeter	$\gamma_s$
Medium	None	None
Cell (Any Color)	25	0.1

**Figure 4.12:** (a) shows the initial condition where approximately equal number of cells are present in each of the segments; (b) shows the final output after 199999 MCS wherein unequal segment width is observed; (c) (Bottom) Parameter Table for the fixed simulation environment for  $T = 40$

junctions. Inspired from [Kicheva et al. 2007](#), the 1D gradient of morphogen model for Dpp-tagged-GFP molecules (morphogen in this case) was simulated in MATLAB to determine the local spatial range of action of Hh-induced Dpp. The spreading of Dpp, produced in the anterior-posterior compartments of the wing epithelium in *Drosophila*, is non-directional and it forms a gradient over space through simple diffusion of molecules. Understanding and integrating the kinetics of such movement into the mechanical model of intrasegmental boundaries can answer questions related to junctional tension due to Hh role. Assuming the parameters shown in Table 3.2, plots were plotted of the concen-

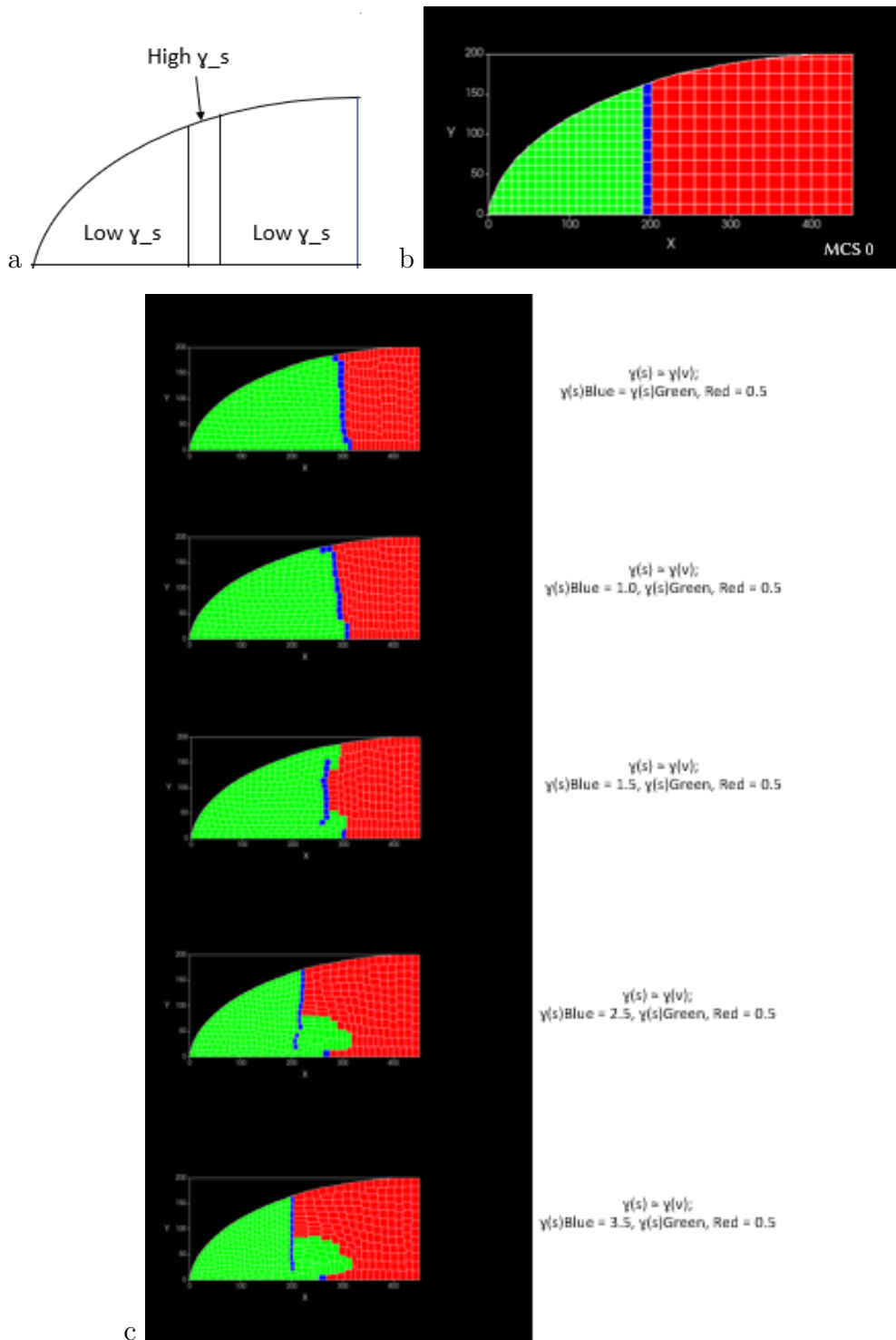


**Figure 4.13:** Schematic of intrasegmental boundaries with band of 3-segments comprising different cell types; (a) show the 3-segment schematic of tissue segments separated by row of highly contractile cells; (b) Initial input with equal cell number in each segment (Green and Red); (c) shows a series of final output (all at MCS 199999) which proves that more contractile cells regulate the movement of segments along with playing a role in cell shapes; All calculations were done at  $T = 40$ .

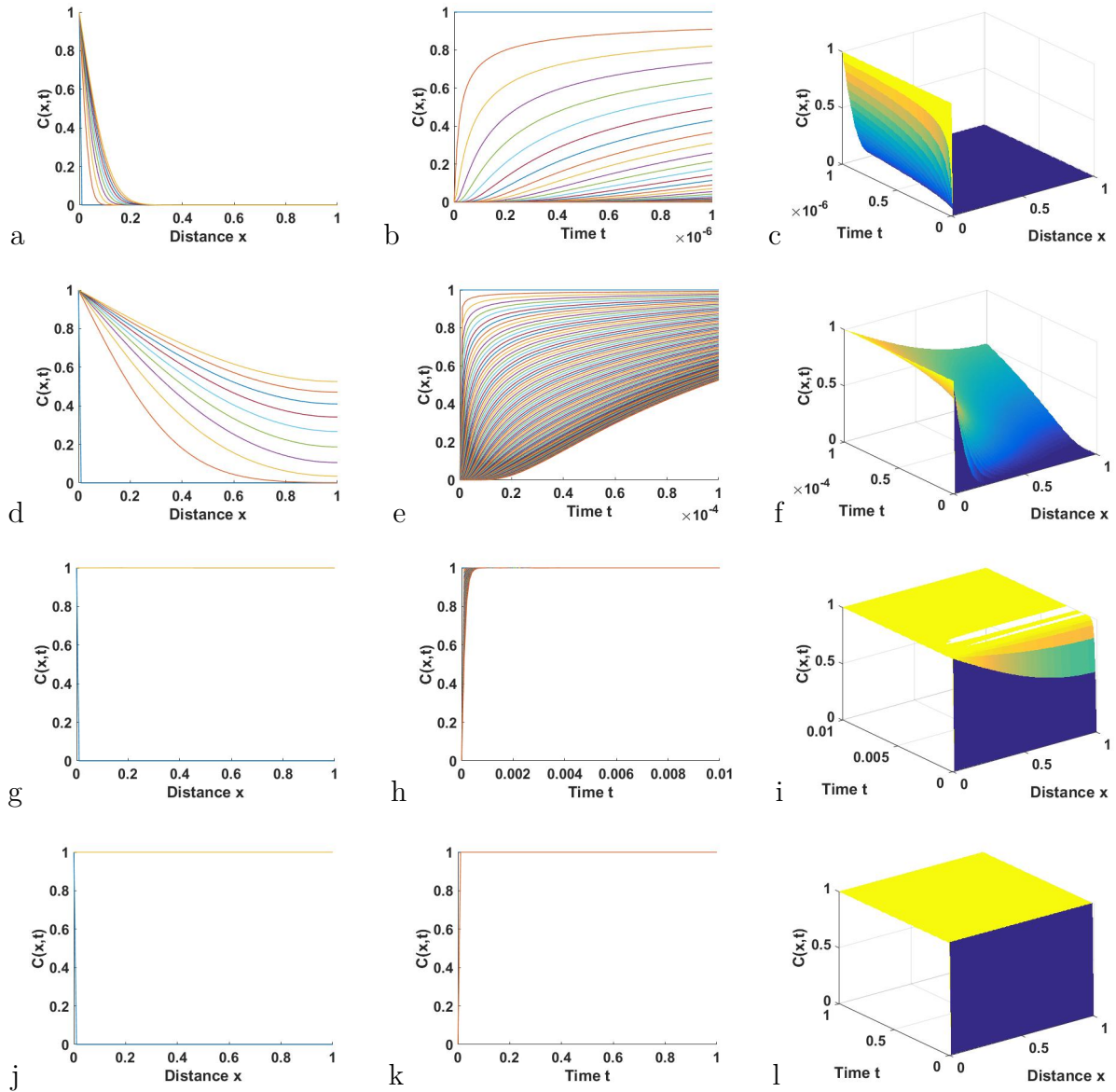


**Figure 4.14:** 1D morphogen (Dpp) gradient simulation over space and time for kinetic analysis at different timescales for fixed length scale; (a)-(l) represents morphogen concentration plots over space, time and spatio-temporal gradient for different maximum simulation times to showcase the effect the timescale of diffusion; Initial condition:  $t=0$  for all  $x$ ; Boundary conditions at  $x=0$  and  $x=L=1$ .

tration of the morphogen over space and time under given initial and boundary conditions which matched with experimental data. Thus an intra-segmental boundary could be created by ascertaining the steady-state solutions to this particular reaction-diffusion of the morphogen and built upon to be included to incorporate with the blue and green cells in the CC3D model.

The principle of morphogen secretion over space and time in 2D was employed by applying a flexible reaction-diffusion solver in CC3D. Certain cells secrete a morphogen according to eqn. 2.7 which affects the other cells to expand and decrease in size depending on the positional value of the cells (Refer Fig. 4.15). This sort of secretion model can be

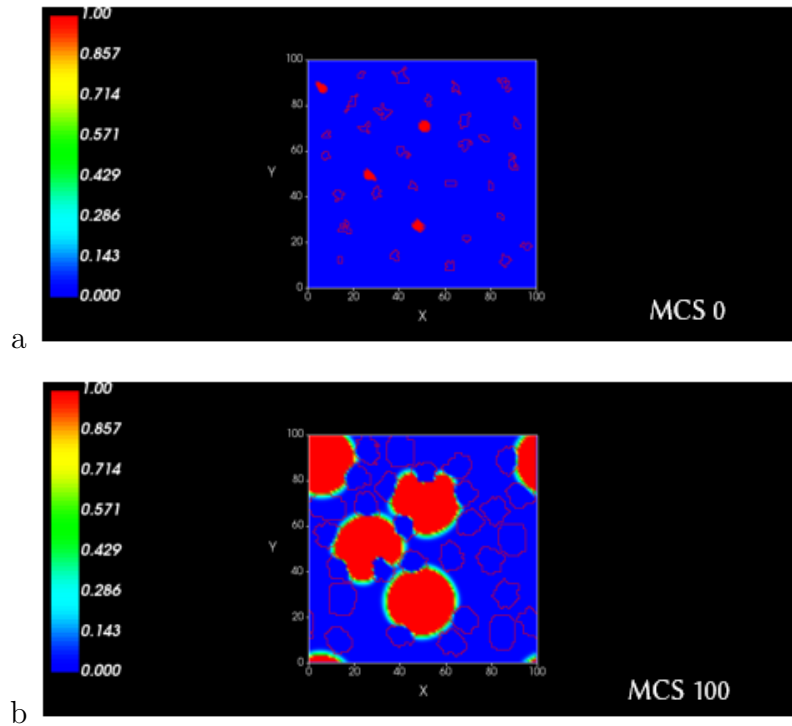


**Figure 4.15:** Reaction-diffusion model of morphogens in secreting cells; Secretion of a morphogen or chemical occurs over time primarily shown by the timesteps MCS 0 ((a)) and MCS 100 ((b)); Continuous secretion coincides with growth of cells and growth of cells is shown to be dependent on the positional data of the neighbouring cells

implemented in the tissue simulation setup to mimic the local Hh and Wg activation along the parasegmental boundaries which in turn should affect the cell sizes and shapes.

# Chapter 5

## Discussion and Conclusion

Polygonal cell shape distribution has been quantified and validated by experimental results. The experimental results, together with the computer simulations, have shown how the biophysical parameters of a CPM scheme can be interpreted into a mechanistic understanding of the forces at play during HI process of *Drosophila* embryogenesis in self-organization of the epithelial tissue. Using only wild-type embryos with GFP marked E-Cadherin, a portion of the epithelia was segmented into polygons with the idea of extracting center of mass co-ordinates and afterward, performing a Voronoi analysis to compare our simulation histogram data with the experimental data. Applying the CPM scheme, a pattern of cell shapes has been recapitulated from only giving in geometrical boundary value conditions showing the importance of proper geometrical considerations. Under equilibrium conditions, the cells in the simulation study are shown to exhibit predominantly pentagonal and hexagonal nature of cell-shapes which is also a consequence of a favourable minimum energy close packing of equal spherical structures (Kepler's Conjecture). The packing efficiency of the hexagonal arrangement of equal shaped objects has been proven to be highest by calculating the space occupied by the objects and dividing it by the volume of the enclosure (Hales 2001). Such shapes are also observed and predicted in the epithelial wing-disc structure of *Drosophila* from Farhadifar *et al.* 2007 and Classen *et al.* 2005 albeit using vertex models.

Thus a CPM model recovers hexagonal cell shapes as predicted from vertex models. But parameter controls for arbitrary values of the input variables are necessary as shown in Table. 3.1.2 keeping in mind the real embryonic data wherein values of surface tension ( $\gamma_v$ ) and especially cortical tension ( $\gamma_s$ ) become important. Cell-cell adhesion driven forces also play a crucial role as is validated by the contact energy variable. Cortical forces arise due to the actomyosin meshwork in the cytoskeleton of individual cells which act collectively to generate tissue-level force (Martin *et al.* 2010). These forces act at the mesoscopic scale and promote active crawling of the epidermis to cover up the head during involution process. Such type of movement is characterized by increased speed in the front or the leading edge of the epidermal tissue and decreased speed in the middle of the embryo. This was quantified after tracking the movement of the denticles. But it is only true for the part of HI process when the head is not covered. Czerniak *et al.* 2016 reports that after the first segment reaches the tip of the head of the embryo, the others gather momentum and distribute accordingly showing increased speeds. Also, the segmentation of the WT embryo with circularity measurement reaffirms the presence of patterned contractile forces which shape the tissue segments and cell shapes. The experimental data of the overexpressed-Hh embryos which shows unequal segment widths



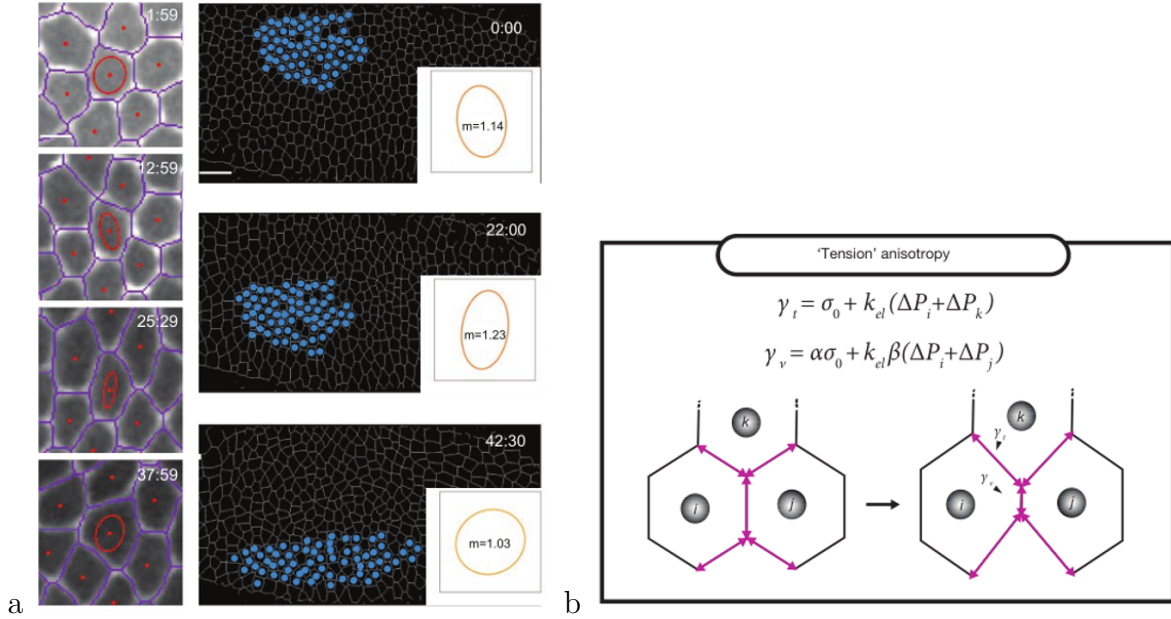


**Figure 5.1:** Anisotropic nature of cortical forces gives rise to elongated cell shapes over space and time in the epithelial tissue characterized in (a); Incorporation of additional terms  $\alpha$  and  $\beta$  in the vertex model of tissue organisation to quantify such anisotropies; Adapted from [Rauzi \*et al.\* 2008](#).

due to the response of all the cells to form a broader band of Wingless-expressing cells in each segment ([Von Ohlen and Hooper 1997](#)). Our simulation setup can recapitulate the overexpression data using simple same contractility of cells or elastic model in the 2D paradigm. Thus the next step would be to input a gradient of contractility (for example, sawtooth ratchet-like gradient) in each segment which can recover the tissue organization in WT embryos. The goal is to integrate a diffusion gradient of active contractility with this geometrical boundary conditions and comment on the tissue organization.

One of the results which need to be studied more carefully and to be incorporated in the model in the future is the anisotropic nature of the cortical forces at play which leads to elongation of specific cells in the tissue more along one direction than the other cells as is observed in [Fig. 4.4\(c\)](#). This has also been reported and incorporated in vertex models using an additional mathematical term defining the anisotropy measure ([Rauzi \*et al.\* 2008](#)). Differential elongation of cells due to anisotropic nature of forces along different axes were quantified and modelled in vertex models by parameterisation of elastic coefficients (Refer [Fig. 5.1](#)). This anisotropy needs to come up in our simulation setup as an inherent emergent property rather than putting something inbuilt into the system. Work remains to be done which includes a quantified comparison study of the tissue segmentation of WT and overexpressed-Hh embryos. The phenotypic difference may reveal the extent of differences in cell shape distribution. Further data analysis on the tissue structure will be able to characterize the differences. A coefficient of variation measure of the length of sides of the polygonal cells after segmentation will be a quantifiable and appropriate measure of the stark differences in cell shapes. The measure can be defined as follows:

$$CV = \frac{\sigma_p}{\mu_p} \quad (5.1)$$

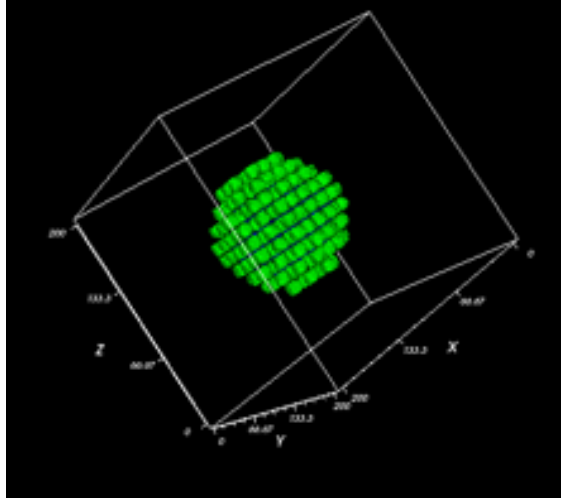


**Figure 5.2:** 3D spherical embryo model in CC3D

where  $\sigma_p$  is the standard deviation of the length of sides of the  $n$ -sided polygon and  $\mu_p$  is the mean of the length of sides of the  $n$ -sided polygons.

There are few published data as to what the dynamics of the tissue morphogenesis is like during the HI stage of *Drosophila* embryogenesis. Such literature reports the antagonistic relations between different signaling molecules leading to the head patterning (Chang *et al.* 2003), and there is the recent Czerniak *et al.* 2016 paper which looks explicitly at the biophysical model of junctional tension within the epidermal segments to answer questions relating to tissue mechanics. This study tries to utilise a framework of a physical description with a fixed geometry of the fly embryo, a gradient of active tensions which can generate moving forces and regulate segment positioning using an agent-based model. We try and formulate a holistic model based on previous and current data, which can incorporate the mechanical principles and biological regulations to answer interesting phenomenon of cell-cell intercalations, tissue deformations, and tissue movements (Guirao and Bellaïche 2017) during crucial developmental processes and wound healing. To recreate a more realistic embryonic tissue environment, a 3D spherical system as shown in Fig. 5.2 has also been worked on as a future perspective for extending our 2D calculations to complex 3D ones. Single layer of cells on the surface of a solid sphere are allowed to simulate which emulate the epithelial tissue on the surface of the *Drosophila* embryo. From the simulation point of view, the mechanical model of junctional tension needs to be coupled with a biochemical feedback loop which affect the contractility measure. Additional studies are required to understand and quantify the tension regulation by coupling between the activation of signaling molecules and the mechanical properties of cells in the epithelial tissue during involution process. Quantitative explanation of such type of regulation will lead to a descriptive and integrative model of developmental forces of tissue remodelling using the Pott's based approach.

# Bibliography

- Aigouy B, Farhadifar R, Staple DB, Sagner A, Röper JC, Jülicher F, Eaton S (2010). Cell Flow Reorients the Axis of Planar Polarity in the Wing Epithelium of *Drosophila*. *Cell* 142(5), 773–786.
- Albert PJ, Schwarz US (2014). Dynamics of cell shape and forces on micropatterned substrates predicted by a cellular Potts model. *Biophysical Journal* 106(11), 2340–2352.
- Andasari V, Roper RT, Swat MH, Chaplain MA (2012). Integrating intracellular dynamics using CompuCell3D and bionetsolver: Applications to multiscale modelling of cancer cell growth and invasion. *PLoS ONE* 7(3).
- Belmonte JM, Swat MH, Glazier JA (2016). Filopodial-Tension Model of Convergent-Extension of Tissues. *PLoS Computational Biology* 12(6).
- Chang T, Shy D, Hartenstein V (2003). Antagonistic relationship between Dpp and EGFR signaling in *Drosophila* head patterning. *Developmental Biology* 263(1), 103–113.
- Classen AK, Anderson KI, Marois E, Eaton S (2005). Hexagonal packing of *Drosophila* wing epithelial cells by the planar cell polarity pathway. *Developmental Cell* 9(6), 805–817.
- Czerniak ND, Dierkes K, D’Angelo A, Colombelli J, Solon J (2016). Patterned Contractile Forces Promote Epidermal Spreading and Regulate Segment Positioning during *Drosophila* Head Involution. *Current Biology* 26(14), 1895–1901.
- David R, Luu O, Damm EW, Wen JWH, Nagel M, Winklbauer R (2014). Tissue cohesion and the mechanics of cell rearrangement. *Development* 141(19), 3672–3682.
- Davidson LA (2012). Epithelial machines that shape the embryo.
- Davies J (2013). Mechanisms of Morphogenesis.
- Farhadifar R, Röper JC, Aigouy B, Eaton S, Jülicher F (2007). The Influence of Cell Mechanics, Cell-Cell Interactions, and Proliferation on Epithelial Packing. *Current Biology* 17(24), 2095–2104.
- Fletcher AG, Osborne JM, Maini PK, Gavaghan DJ (2013). Implementing vertex dynamics models of cell populations in biology within a consistent computational framework.
- Graner F, Glazier J (1992). Simulation of biological cell sorting using a two-dimensional extended Potts model. *Physical review letters* 69(13), 2013–2016.

- Guillot C, Lecuit T (2013). Mechanics of Epithelial Tissue Homeostasis and Morphogenesis. *Science* 340(6137), 1185–1189.
- Guirao B, Bellaïche Y (2017). Biomechanics of cell rearrangements in *Drosophila*.
- Hales TC (2001). The honeycomb conjecture. *Discrete and Computational Geometry* 25(1), 1–22.
- Ingham PW, McMahon AP (2001). Hedgehog signaling in animal development: Paradigms and principles.
- Karsenti E (2008). Self-organization in cell biology: a brief history. *Nature Reviews Molecular Cell Biology* 9(3), 255–262.
- Kicheva A, Pantazis P, Bollenbach T, Kalaidzidis Y, Bittig T, Jülicher F, González-Gaitán M (2007). Kinetics of morphogen gradient formation. *Science* 315(5811), 521–525.
- Lecuit T, Lenne PF (2007). Cell surface mechanics and the control of cell shape, tissue patterns and morphogenesis. *Nature reviews Molecular cell biology* 8(8), 633–44.
- Li X, Deng W, Nail CD, Bailey SK, Kraus MH, Ruppert JM, Lobo-Ruppert SM (2006). Snail induction is an early response to Gli1 that determines the efficiency of epithelial transformation. *Oncogene* 25(4), 609–621.
- Magno R, Grieneisen VA, Marée AF (2015). The biophysical nature of cells: Potential cell behaviours revealed by analytical and computational studies of cell surface mechanics. *BMC Biophysics* 8(1).
- Marée AFM, Grieneisen VA, Edelstein-Keshet L (2012). How cells integrate complex stimuli: The effect of feedback from phosphoinositides and cell shape on cell polarization and motility. *PLoS Computational Biology* 8(3).
- Martin AC, Gelbart M, Fernandez-Gonzalez R, Kaschube M, Wieschaus EF (2010). Integration of contractile forces during tissue invagination. *Journal of Cell Biology* 188(5), 735–749.
- Müller G, Newman S (2003). Origination of organismal form: beyond the gene in developmental and evolutionary biology.
- Niculescu I, Textor J, de Boer RJ (2015). Crawling and Gliding: A Computational Model for Shape-Driven Cell Migration. *PLoS Computational Biology* 11(10).
- Okabe A, Boots B, Sugihara K, Chiu SN, Kendall DG (2008). Definitions and Basic Properties of Voronoi Diagrams. In *Spatial Tessellations*, 43–112.
- Procacci A, Scoppola B, Scoppola E (2016). Probabilistic Cellular Automata for Low-Temperature 2-d Ising Model. *Journal of Statistical Physics* 165(6), 991–1005.
- Rauzi M, Verant P, Lecuit T, Lenne PF (2008). Nature and anisotropy of cortical forces orienting *Drosophila* tissue morphogenesis. *Nature Cell Biology* 10(12), 1401–1410.
- Salbreux G, Charras G, Paluch E (2012). Actin cortex mechanics and cellular morphogenesis.

- Sanson B (2001). Generating patterns from fields of cells: Examples from *Drosophila* segmentation.
- Sbalzarini IF, Koumoutsakos P (2005). Feature point tracking and trajectory analysis for video imaging in cell biology. *Journal of Structural Biology* 151(2), 182–195.
- Schindelin J, Arganda-Carreras I, Frise E, Kaynig V, Longair M, Pietzsch T, Preibisch S, Rueden C, Saalfeld S, Schmid B, Tinevez JY, White DJ, Hartenstein V, Eliceiri K, Tomancak P, Cardona A (2012). Fiji: An open-source platform for biological-image analysis.
- Solon J, Kaya-Çopur A, Colombelli J, Brunner D (2009). Pulsed Forces Timed by a Ratchet-like Mechanism Drive Directed Tissue Movement during Dorsal Closure. *Cell* 137(7), 1331–1342.
- St Johnston D, Sanson B (2011). Epithelial polarity and morphogenesis.
- Steinberg MS (2007). Differential adhesion in morphogenesis: a modern view.
- Swat MH, Thomas GL, Belmonte JM, Shirinifard A, Hmeljak D, Glazier JA (2012). Multi-Scale Modeling of Tissues Using CompuCell3D. *Methods in Cell Biology* 110, 325–366.
- The Mathworks Inc (2016). MATLAB - MathWorks.
- Thompson DW (1942). On growth and form.
- Turner S, Sherratt JA, Painter KJ, Savill NJ (2004). From a discrete to a continuous model of biological cell movement. *Phys Rev E* 69(2), 21910.
- VanHook A, Letsou A (2008). Head involution in *Drosophila*: Genetic and morphogenetic connections to dorsal closure.
- von Dassow G, Meir E, Munro EM, Odell GM (2000). The segment polarity network is a robust developmental module. *Nature* 406(6792), 188–192.
- Von Ohlen T, Hooper JE (1997). Hedgehog signaling regulates transcription through Gli/Ci binding sites in the wingless enhancer. *Mechanisms of Development* 68(1-2), 149–156.